This version of the ESI published on 23 Aug 2024 replaces the original version published on 24 July 2024. The changes made do not affect the scientific content.

Electronic Supplementary Information

Observation of ferroelectric behaviour in non-symmetrical cholesterol-based bent-shaped dimers

Vidhika Punjani,[a,b] Golam Mohiuddin,[a,c] Susanta Chakraborty,[d] Priyanta Barman,[d] Anshika Baghla,[a] Madhu Babu Kanakala,[e] Malay Kumar Das,[d] Channabasaveshwar Yelamaggad[e,f,g] and Santanu Kumar Pal[a]*

[a]Department of Chemical Sciences, Indian Institute of Science Education and Research (IISER) Mohali, Sector 81, Knowledge City, Manauli-140306, India.

[b]Centre of Molecular and Macromolecular Studies, Polish Academy of Sciences, 90-363 Łódź, Poland

[c]Department of Chemistry, University of Science & Technology Meghalaya, Ri-Bhoi, Meghalaya 793101, India.

[d]Department of Physics, University of North Bengal, Siliguri-734 013, India.

[e]Centre for Nano and Soft Matter Sciences, Bengaluru, 560013, India

[f]Department of Chemistry, Manipal Institute of Technology, Manipal Academy of Higher Education, Manipal – 576104, India.

[g]SJB Institute of Technology, Health & Education City, Kengeri, Bengaluru – 560060, India

E-mail: skpal@iisermohali.ac.in, santanupal.20@gmail.com

Table of contents:

This version of the ESI published on 23 Aug 2024 replaces the original version published on 24 July 2024. The changes made do not affect the scientific content.

1. Synthesis

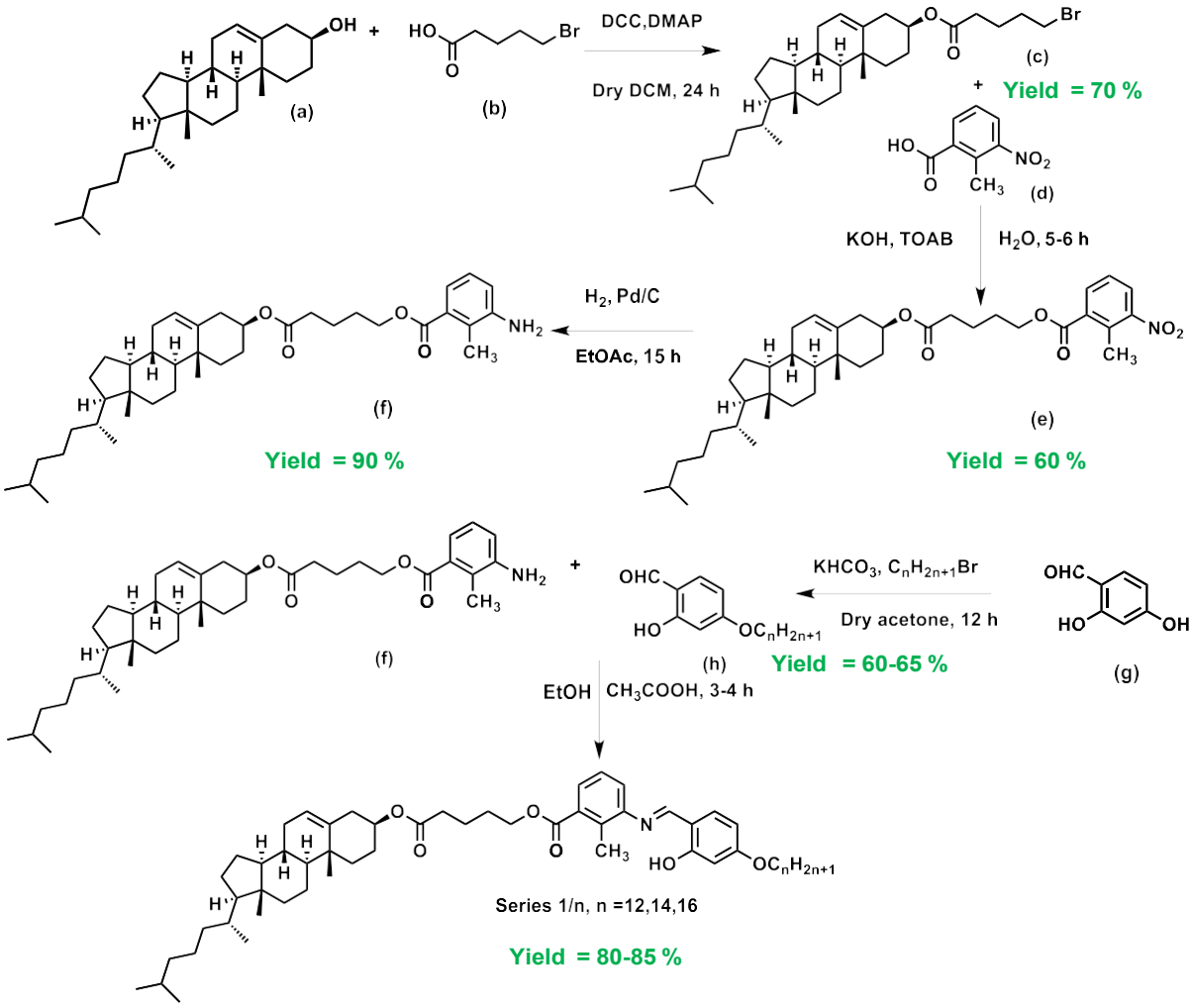

Scheme S1. Synthetic scheme for the synthesis of the desired non-symmetrical cholesterol-based dimers.

Synthesis of c, (3S,8S,9S,10R,13R,14S,17R)-10,13-dimethyl-17-((R)-6-methylheptan-2-yl)-2,3,4,7,8,9,10,11,12,13,14,15,16,17-tetradecahydro-1H-cyclopenta[a]phenanthren-3-yl 5-bromopentanoate

Scheme S1 shows the synthetic formation of compound **c**. The first step involves the coupling of the -OH group of the cholesterol moiety and -COOH group of the 5-bromovaleric acid leading to the formation of an ester linkage between the cholesterol and 5-bromovaleric acid. This reaction is known as Steglich esterification. The following procedure has been reported earlier and is reproduced below as follows[1,2]:

This version of the ESI published on 23 Aug 2024 replaces the original version published on 24 July 2024. The changes made do not affect the scientific content.

"5-bromovaleric acid (**b**, 1 equivalent) was dissolved in 50 mL of dry dichloromethane (DCM) in a two-neck round-bottomed flask under inert conditions in the presence of N_2 gas. Further, the catalytic amount of 4-dimethylaminopyridine (DMAP) was followed by the addition of N, N'-dicyclohexylcarbodiimide (DCC, 1.25 equivalent). Cholesterol (**a**, 1.1 equivalent) was then added and the reaction mixture was stirred for 24 hours. After 24 hours, the precipitate (Dicyclohexylurea) was filtered off and the rotatory evaporation of the filtrate gave the crude reaction mixture. The product (**c**) was obtained by carrying out the column chromatography of the crude reaction mixture using silica gel of 60-120 and by eluting it with a mixture of hexane and ethyl acetate (v/v, 100:1). The product (c) is obtained as a white solid." Yield = 70 %.

Synthesis of e, 5-(((3S,8S,9S,10R,13R,14S,17R)-10,13-dimethyl-17-((R)-6-methylheptan-2-yl)-2,3,4,7,8,9,10,11,12,13,14,15,16,17-tetradecahydro-1H-cyclopenta[a]phenanthren-3-yl)oxy)-5-oxopentyl 2-methyl-3-nitrobenzoate

Scheme S1 shows the synthetic formation of compound **e**. For the synthesis of the intermediate **e**, an ester linkage is formed between the compound **c** and **d** (2-methyl-3-nitrobenzoic acid).[3]

1 equivalent of compound **d** was dissolved in aqueous KOH (1 equivalent) and the reaction mixture was stirred for 15 minutes. To that solution, compound **c (** 2 equivalent**)** was added and the catalytic amount of tetraoctylammonium bromide (TOAB) was added. The reaction mixture was vigorously stirred for 5-6 hours and then cooled to room temperature. Chloroform was used to extract the reaction mixture. Further, brine was used to wash the organic layer and then the organic layer was dried with sodium sulphate. The reaction mixture was purified by column chromatography (silica gel, 60-120 mesh) and eluting with hexane and ethyl acetate (v/v, 100:4).[3] The product **e** was obtained as a white solid. Yield = 60 %., **^{1}H NMR (400 MHz, Chloroform-*d*, δ in ppm)** δ = 7.98 (dd, *J* = 7.8, 1.4 Hz, 1H, Ar-H), 7.84 (dq, *J* = 8.2, 1.7 Hz, 1H, , Ar-H), 7.38 (t, *J* = 8.0 Hz, 1H, , Ar-H), 5.36 (dd, *J* = 4.4, 2.4 Hz, 1H, -CH=C- in cholesteryl), 4.66-4.59 (m, 1H, -CH-O- in cholesteryl), 4.35 (t, *J* = 5.8 Hz, 2H, -OCH_2-), 2.62 (s, 3H, -CH_3 of central aromatic core), 2.36 (t, *J* = 6.8 Hz, 2H), 2.30 (d, *J* = 8.0 Hz, 2H), 2.03-1.93 (m, 2H), 1.87-1.76 (m, 7H), 1.55-0.84 (33H, extensive coupling in cholesteryl, spacer unit and alkyl chains), 0.67 (s, 3H), **^{13}C NMR (101 MHz, Chloroform-*d*, δ in ppm)** δ = 172.56, 166.41, 151.95, 139.54, 133.59, 133.54, 132.99, 126.65, 126.40, 122.75, 74.02, 65.28, 56.66, 56.11, 49.99, 42.29, 39.70, 39.50, 38.14, 36.95, 36.57, 36.17, 35.79, 34.04, 31.89, 31.83, 28.23, 28.03, 28.01, 27.80, 24.28, 23.82, 22.83, 22.57, 21.61, 21.02, 19.31, 18.71, 16.25, 11.85.

This version of the ESI published on 23 Aug 2024 replaces the original version published on 24 July 2024. The changes made do not affect the scientific content.

Synthesis of f, 5-(((3S,8S,9S,10R,13R,14S,17R)-10,13-dimethyl-17-((R)-6-methylheptan-2-yl)-2,3,4,7,8,9,10,11,12,13,14,15,16,17-tetradecahydro-1H-cyclopenta[a]phenanthren-3-yl)oxy)-5-oxopentyl 3-amino-2-methylbenzoate

Scheme S1 shows the synthetic formation of compound **f**. The following procedure has been reported earlier and is reproduced below as follows[1,2]:

"This step involves the reduction of the -NO_2 group in intermediate **e** via hydrogenation. The compound **e** was dissolved in a minimum amount of ethyl acetate. To that, 5 wt % of Palladium on activated charcoal (Pd/C) was added and the reaction mixture was stirred for 15 hours under H_2 atmosphere. After 15 hours, the reaction mixture was filtered to remove the catalyst and the pure product (**f**) was collected after rotatory evaporation of the filtrate." Yield = 90 %, **^{1}H NMR (400 MHz, Chloroform-*d*, δ in ppm)** δ = 7.21 (dd, *J* = 7.7, 1.3 Hz, 1H, Ar-H), 7.05 (t, *J* = 7.8 Hz, 1H, Ar-H), 6.81 (dd, *J* = 7.9, 1.3 Hz, 1H, Ar-H), 5.37 (dd, *J* = 4.9, 1.9 Hz, 1H, -CH=C- in cholesteryl), 4.66-4.58 (m, 1H, -CH-O- in cholesteryl), 4.30 (m, J = 3.7, 3.2 Hz, 2H, -OCH_2-), 3.74 (s, 2H, -NH_2), 2.37-2.30 (m, 7H), 2.03-1.93 (m, 2H), 1.88-1.77 (m, 7H), 1.64-0.85 (33H, extensive coupling in cholesteryl, spacer unit and alkyl chains), 0.68 (s, 3H), **^{13}C NMR (101 MHz, Chloroform-*d*, δ in ppm)** δ = 172.74, 168.68, 145.47, 139.64, 131.81, 126.09, 122.87, 122.68, 120.35, 118.14, 73.95, 64.37, 56.68, 56.12, 50.01, 42.31, 39.72, 39.52, 38.15, 36.98, 36.60, 36.19, 35.81, 34.18, 31.91, 31.85, 28.25, 28.16, 28.03, 27.81, 24.30, 23.84, 22.85, 22.59, 21.73, 21.03, 19.33, 18.73, 13.91, 11.87.

Synthesis of h, 4-n-alkoxy-2-hydroxybenzaldehyde

Scheme S1 shows the synthetic formation of compound **h**. The following procedure has been reported earlier and is reproduced below as follows[1,2]:

"2, 4-dihydroxybenzaldehyde (**g**, 1 equivalent), $KHCO_3$ (1 equivalent), and a catalytic amount of KI was added in 250 mL of dry acetone in two neck round-bottomed flask. Further, 1 equivalent of 1-bromoalkane was added and the reaction mixture was stirred for 12 hours. After 12 hours, the precipitate of $KHCO_3$ was removed and the filtrate was collected. The rotatory evaporation of the filtrate gave the reaction mixture, and the product (**h**) was obtained by column chromatography using hexane and ethyl acetate as eluent (v/v, 100:1). The product was obtained as a pale-yellow liquid. Yield = 60-65%

The above procedure was used to synthesize the homologues (n = 12, 14, 16) by the above procedure.

This version of the ESI published on 23 Aug 2024 replaces the original version published on 24 July 2024. The changes made do not affect the scientific content.

Synthesis of 1/n, 5-(((3S,8S,9S,10R,13R,14S,17R)-10,13-dimethyl-17-((R)-6-methylheptan-2-yl)-2,3,4,7,8,9,10,11,12,13,14,15,16,17-tetradecahydro-1H-cyclopenta[a]phenanthren-3-yl)oxy)-5-oxopentyl 3-(((E)-4-(alkoxy)-2-hydroxybenzylidene)amino)-2-methylbenzoate

Scheme S1 shows the synthetic formation of compound **1/n**. The following procedure has been reported earlier and is reproduced below as follows[1,2]:

This step involves the formation of a Schiff base linkage between **f** and **h**. The final compound was prepared by refluxing an ethanolic solution of **f** and **h** with a few drops of acetic acid for 3 hours. The final product precipitates out and is purified by recrystallization. The final product **1/n** was obtained as a pale-yellow solid. Yield = 80-85 %. The alkyl chains were varied from n = 12 to n =16 and final compounds **1/12**, **1/14**, and **1/16** were prepared. ^{1}H NMR, ^{13}C NMR, HRMS, UV-vis, and ATR for all the final compounds are presented below.

Compound 1/12

UV-vis: 287 nm, 338 nm, **ATR:** -C-H- stretch at 2853 cm^{-1}, 2925 cm^{-1}, C=O stretching band of ester at 1726 cm^{-1}, HC=N- stretching of imine at 1612 cm^{-1}, **HRMS (ESI-MS):** m/z calculated for $C_{59}H_{90}NO_6$ $[M+H]^+$: 908.6768; found: 908.6793, **^{1}H NMR (400 MHz, Chloroform-*d*, δ in ppm)** δ = 13.56 (s, 1H, -OH), 8.41 (s, 1H, -CH=N-), 7.69 (d, *J* = 7.7 Hz, 1H, Ar-H), 7.30-7.27 (m, 2H, Ar-H), 7.17 (d, *J* = 7.8 Hz, 1H, Ar-H), 6.50 (dd, *J* = 7.2, 2.3 Hz, 2H, Ar-H), 5.37 (d, *J* = 5.0 Hz, 1H, -CH=C- in cholesteryl), 4.65-4.58 (m, 1H, -CH-O- in cholesteryl), 4.33 (t, *J* = 5.7 Hz, 2H, -OCH_2-), 4.00 (t, *J* = 6.4 Hz, 2H, -OCH_2-), 2.57 (s, 3H, -CH_3 in central aromatic core), 2.38-2.29 (m, 4H), 2.03-1.98 (m, 2H), 1.87-1.76 (m, 9H), 1.50-0.85 (54H, extensive coupling in cholesteryl, spacer unit and alkyl chains), 0.67 (s, 3H, -CH_3), **^{13}C NMR (101 MHz, Chloroform-d, δ in ppm)** δ = 172.71, 167.99, 163.79, 163.71, 162.40, 149.23, 139.62, 133.59, 132.97, 132.01, 127.76, 126.42, 122.69, 121.64, 112.99, 107.71, 101.51, 73.98, 68.31, 64.64, 56.68, 56.12, 50.00, 42.31, 39.73, 39.53, 38.15, 36.98, 36.59, 36.19, 35.82, 34.16, 31.95, 31.91, 31.85, 29.69, 29.67, 29.63, 29.59, 29.39, 29.08, 28.26, 28.15, 28.04, 27.82, 26.01, 24.30, 23.85, 22.86, 22.73, 22.59, 21.75, 21.04, 19.33, 18.73, 15.41, 14.17, 11.87.

Compound 1/14

UV-vis: 287 nm, 338 nm, **ATR:** -C-H- stretch at 2853 cm^{-1}, 2925 cm^{-1}, C=O stretching band of ester at 1726 cm^{-1}, HC=N stretching of imine at 1612 cm^{-1}, **HRMS (ESI-MS):** m/z

This version of the ESI published on 23 Aug 2024 replaces the original version published on 24 July 2024. The changes made do not affect the scientific content.

calculated for $C_{61}H_{94}NO_6$ $[M+H]^+$: 936.7081; found: 936.7058, **^{1}H NMR (400 MHz, Chloroform-*d*, , δ in ppm)** δ = 13.58 (s, 1H, -OH), 8.41 (s, 1H, -CH=N-), 7.69 (d, *J* = 7.7 Hz, 1H, Ar-H), 7.32-7.27 (m, 2H, Ar-H), 7.17 (d, *J* = 7.7 Hz, 1H), 6.51-6.49 (m, 2H, Ar-H), 5.37 (d, J = 5.0 Hz, 1H, -CH=C- in cholesteryl), 4.66-4.58 (m, 1H, -CH-O- in cholesteryl), 4.33 (t, 2H, *J* = 5.7 Hz , -OCH_2-), 4.00 (t, J = 6.6 Hz, 2H, -OCH_2-), 2.57 (s, 3H, -CH_3 in central aromatic core), 2.38-2.30 (m, 4H), 2.02-1.94 (m, 2H), 1.87-1.77 (m, 9H), 1.53-0.85 (58 H, extensive coupling in cholesteryl, spacer unit and alkyl chains), 0.67 (s, 3H, -CH_3), **^{13}C NMR (101 MHz, Chloroform-*d*, , δ in ppm)** δ = 172.67, 167.95, 163.79, 163.72, 162.38, 149.23, 139.61, 133.58, 132.98, 132.01, 127.76, 126.41, 122.66, 121.61, 113.00, 107.69, 101.52, 73.96, 68.30, 64.62, 56.68, 56.13, 50.01, 42.31, 39.73, 39.53, 38.15, 36.98, 36.59, 36.20, 35.81, 34.15, 31.95, 31.91, 31.85, 29.72, 29.69, 29.62, 29.59, 29.39, 29.08, 28.25, 28.15, 28.03, 27.82, 26.00, 24.29, 23.85, 22.85, 22.72, 22.59, 21.75, 21.04, 19.32, 18.73, 15.37, 14.16, 11.87.

Compound 1/16

UV-vis: 287 nm, 338 nm, **ATR:** -C-H- stretch at 2852 cm^{-1}, 2926 cm^{-1}, C=O stretching band of ester at 1726 cm^{-1}, HC=N stretching of imine at 1612 cm^{-1}, **HRMS (ESI-MS):** m/z calculated for $C_{63}H_{98}NO_6$ $[M+H]^+$: 964.7378; found: 964.7357, **^{1}H NMR (400 MHz, Chloroform-*d*, δ in ppm)** δ = 13.58 (s, 1H, -OH), 8.41 (s, 1H, -CH=N-), 7.69 (d, *J* = 7.3 Hz, 1H, Ar-H), 7.31-7.27 (m, 2H, Ar-H), 7.17 (d, *J* = 7.7 Hz, 1H, Ar-H), 6.51-6.49 (m, 2H, Ar-H), 5.37 (d, *J* = 4.9 Hz, 1H, -CH=C- in cholesteryl), 4.65-4.59 (m, 1H, -CH-O- in cholesteryl), 4.34 (t, *J* = 5.5 Hz, 2H, -OCH_2-), 4.00 (t, *J* = 6.6 Hz, 2H, -OCH_2-), 2.57 (s, 3H, -CH_3 of central aromatic core), 2.38-2.30 (m, 4H), 2.00 (d, *J* = 13.2 Hz, 2H), 1.86-1.76 (m, 9H), 1.50-1.42 (m, 7H), 1.32-0.85 (55H, extensive coupling in cholesteryl, spacer unit and alkyl chains), 0.67 (s, 3H, -CH_3), **^{13}C NMR (101 MHz, Chloroform-*d*, δ in ppm)** δ = 172.69, 167.98, 163.79, 163.72, 162.39, 149.23, 139.61, 133.59, 132.99, 132.00, 127.77, 126.42, 122.69, 121.63, 112.99, 107.70, 101.51, 73.97, 68.30, 64.64, 56.68, 56.12, 50.00, 42.31, 39.73, 39.53, 38.15, 36.98, 36.59, 36.20, 35.82, 34.16, 31.96, 31.91, 31.85, 29.74, 29.70, 29.64, 29.60, 29.41, 29.09, 28.26, 28.16, 28.04, 27.82, 26.02, 24.30, 23.85, 22.87, 22.74, 22.60, 21.75, 21.04, 19.34, 18.74, 15.41, 14.18, 11.88.

This version of the ESI published on 23 Aug 2024 replaces the original version published on 24 July 2024. The changes made do not affect the scientific content.

2. Chemical Characterization

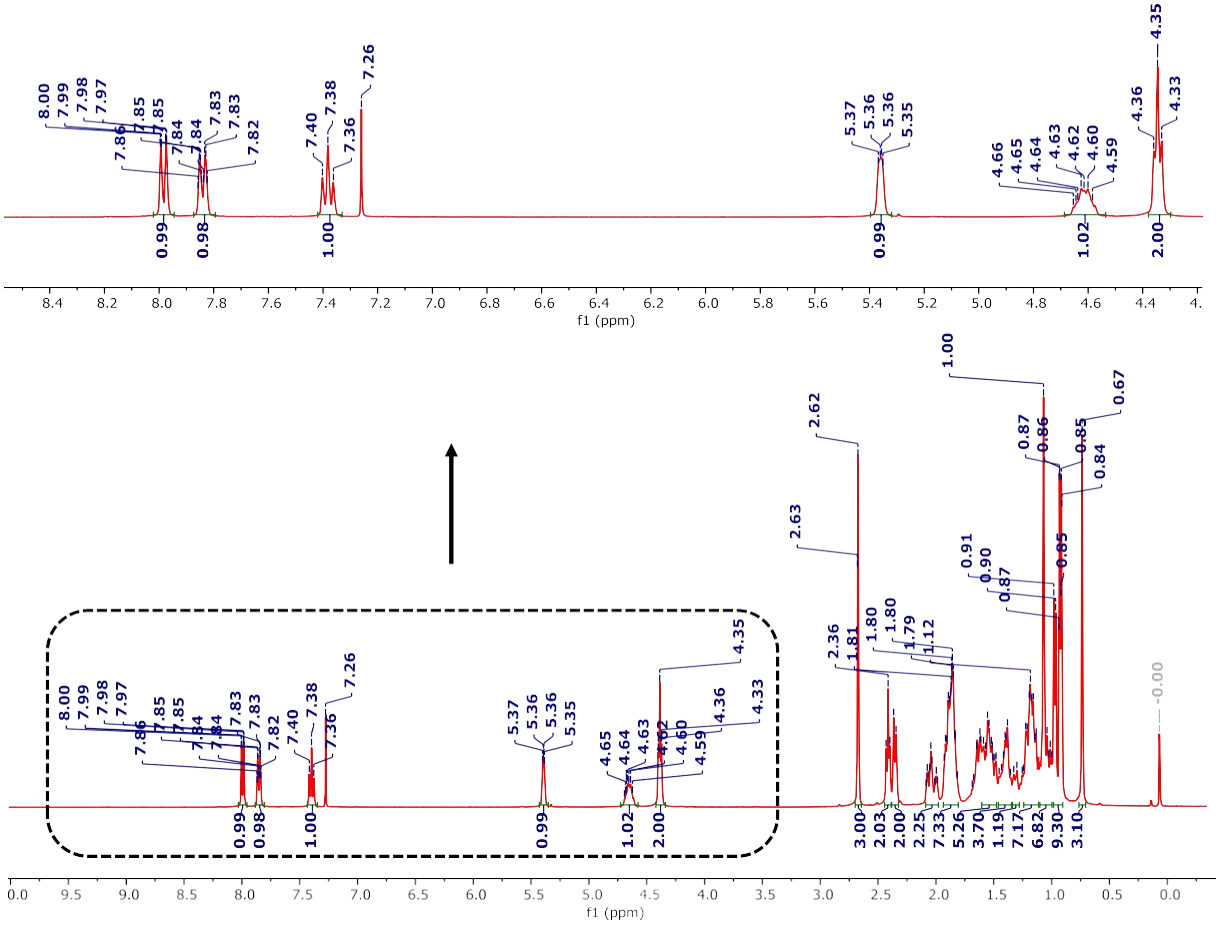

Fig. S1 ^{1}H NMR spectrum of compound **e**.

This version of the ESI published on 23 Aug 2024 replaces the original version published on 24 July 2024. The changes made do not affect the scientific content.

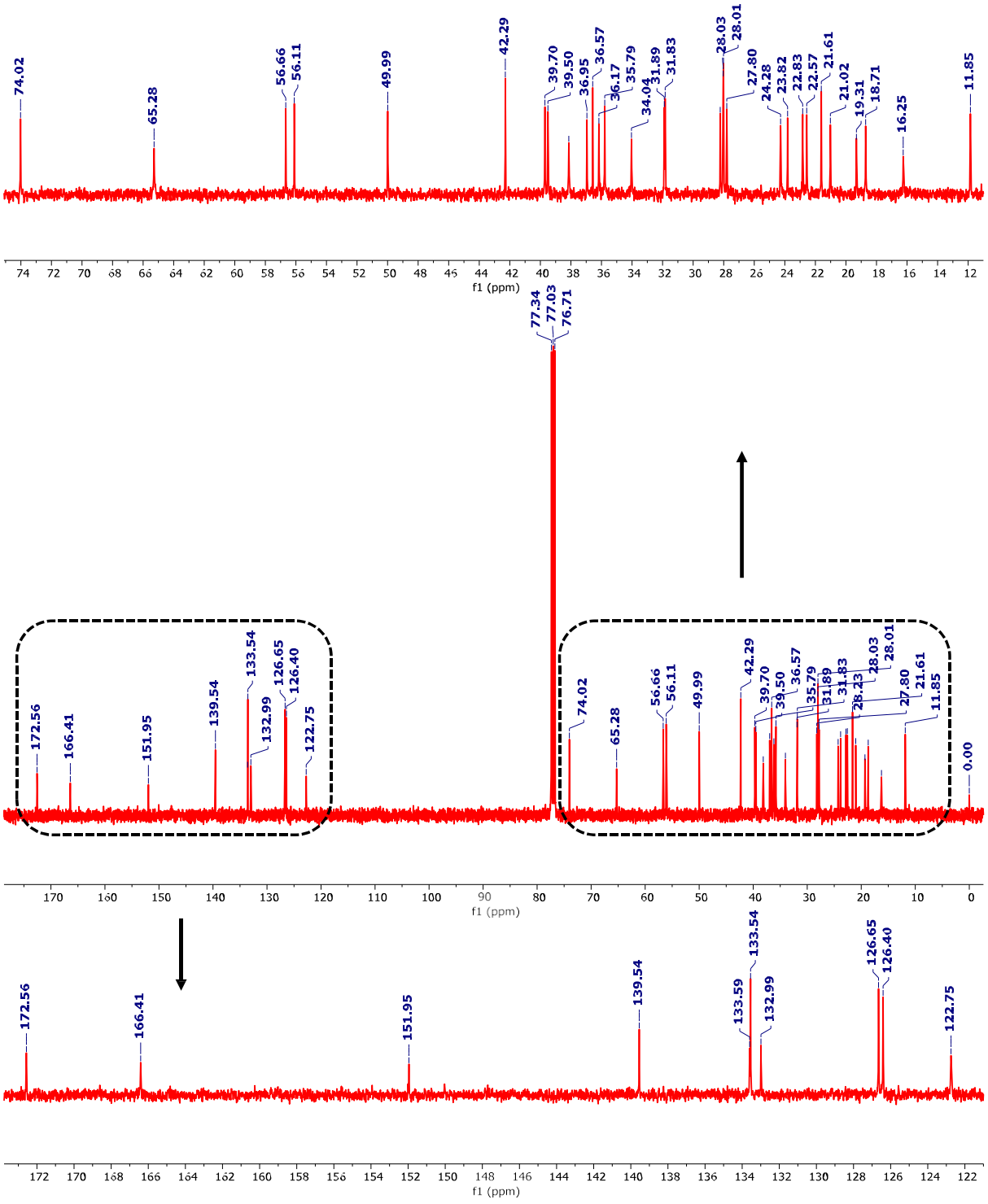

Fig. S2 ^{13}C NMR spectrum of compound **e**.

This version of the ESI published on 23 Aug 2024 replaces the original version published on 24 July 2024. The changes made do not affect the scientific content.

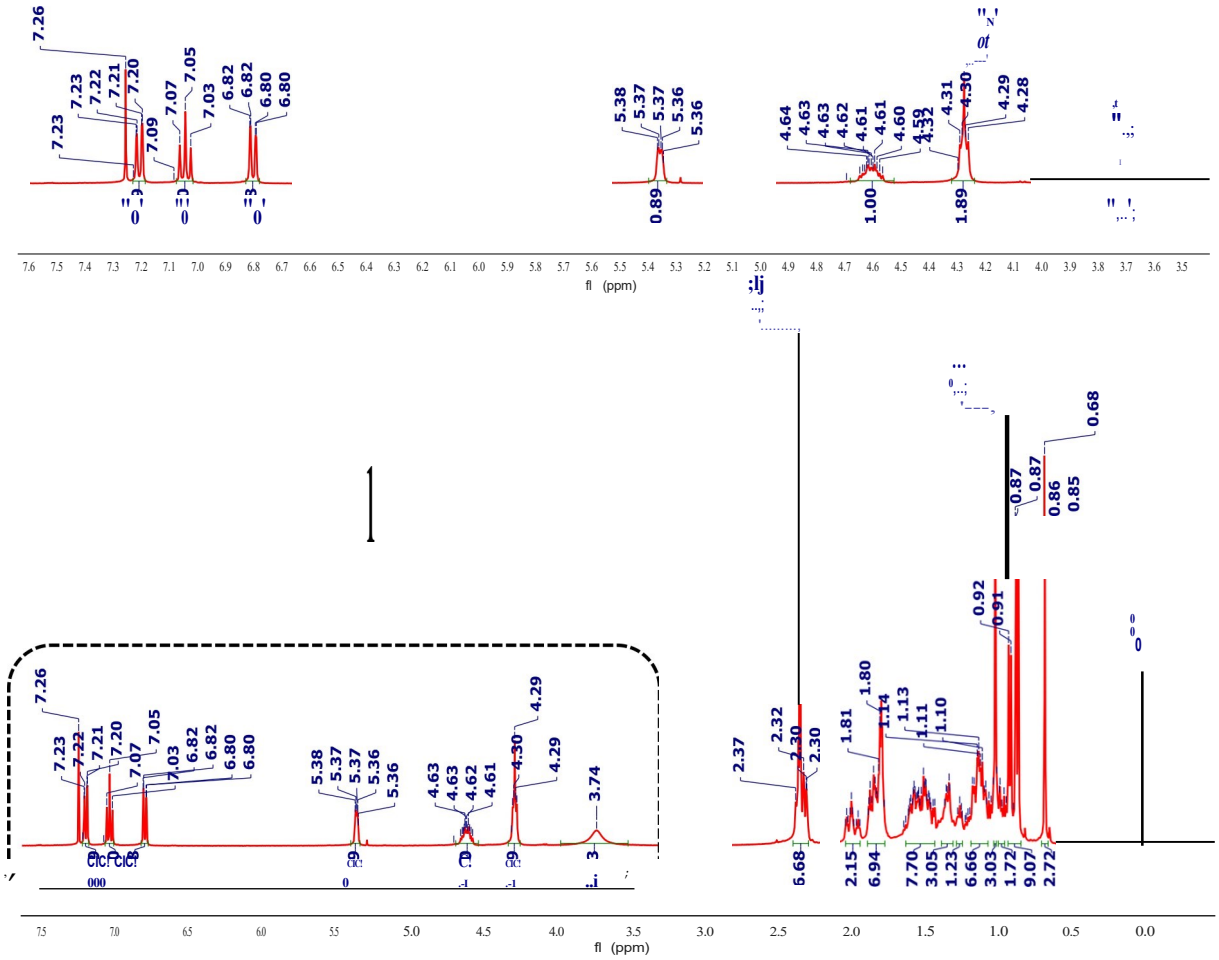

Fig. S3 ^{1}H NMR spectrum of compound **f**.

This version of the ESI published on 23 Aug 2024 replaces the original version published on 24 July 2024. The changes made do not affect the scientific content.

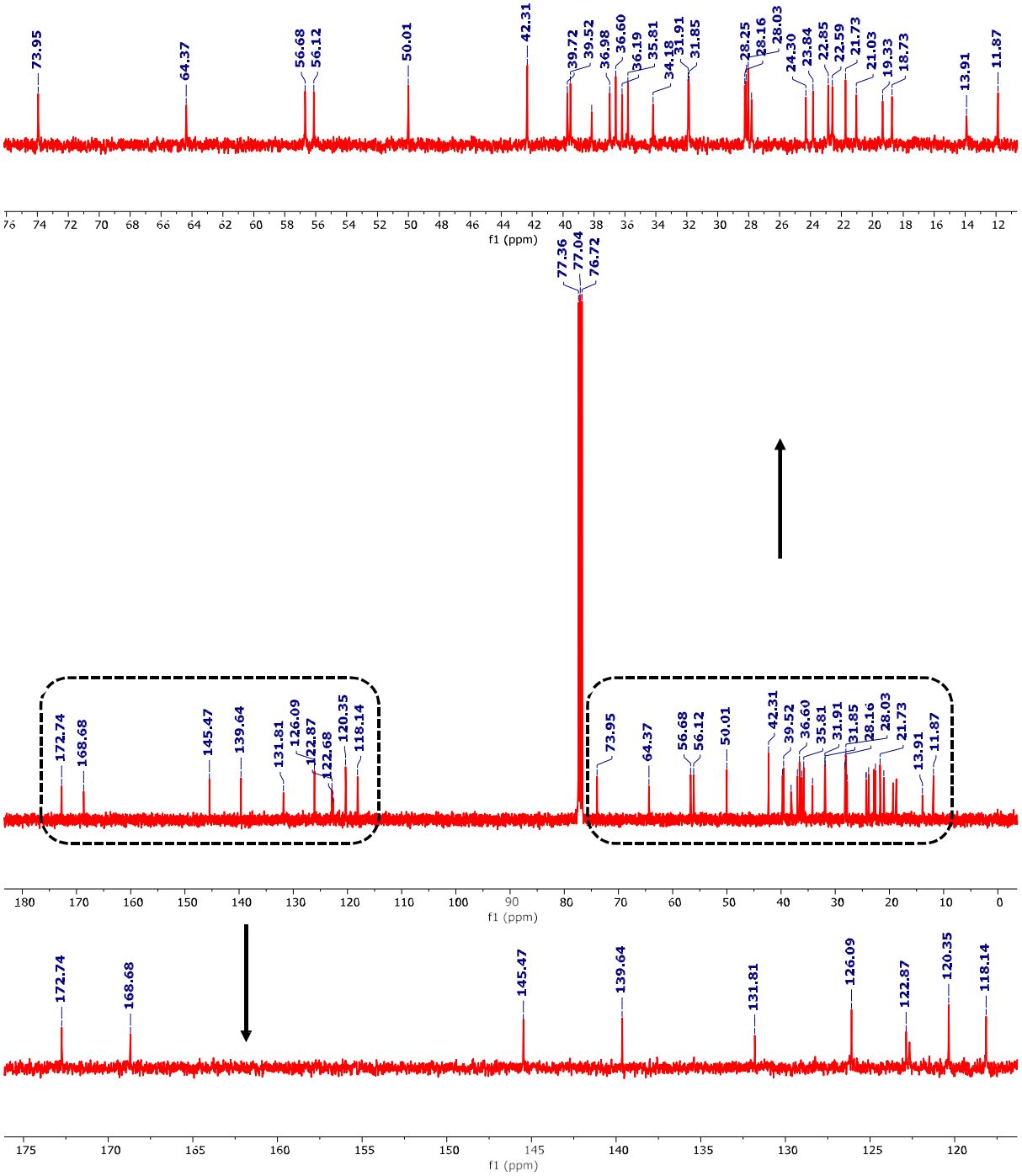

Fig. S4 ^{13}C NMR spectrum of compound **f**.

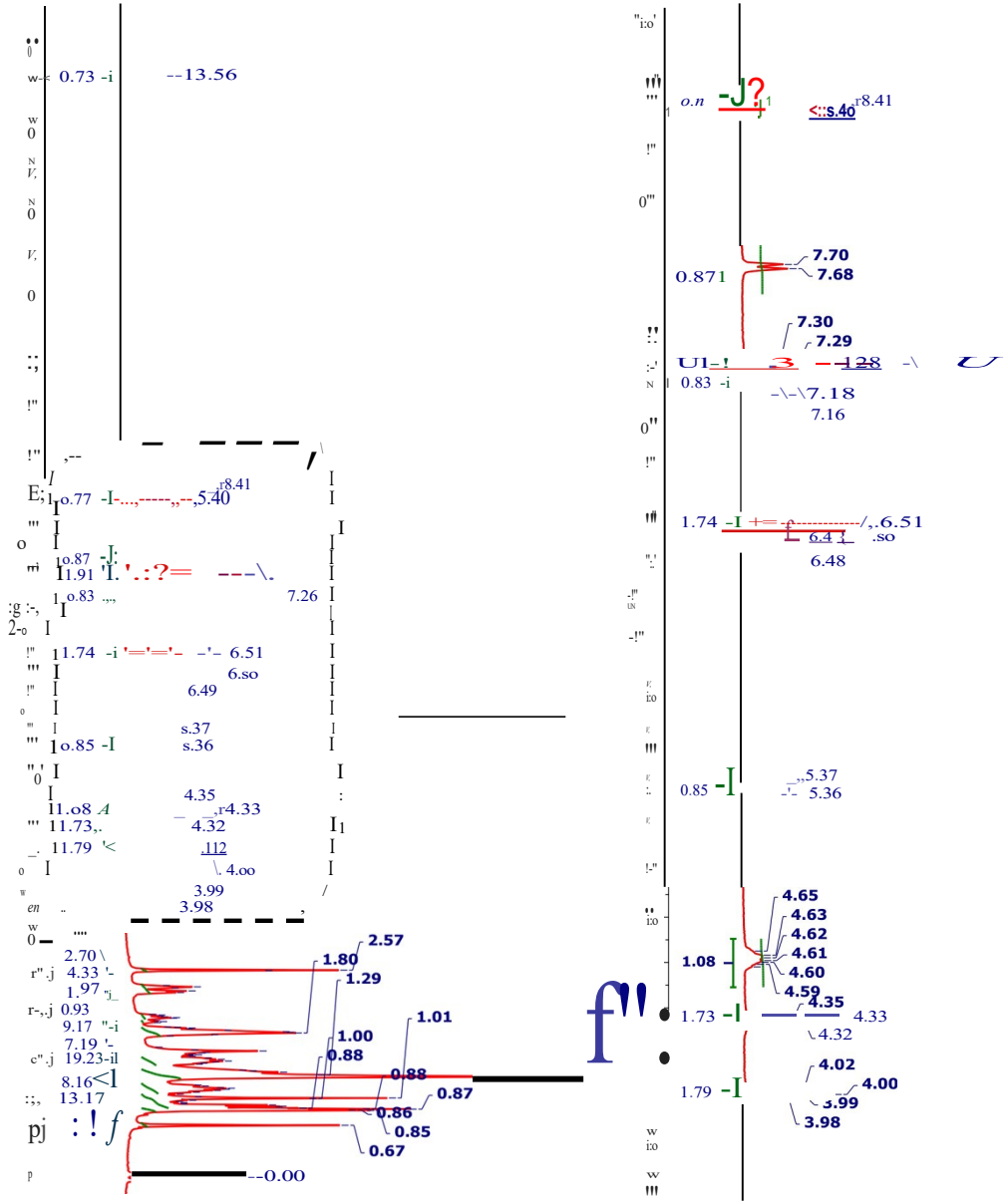

Fig. S5 ^{1}H NMR spectrum of compound **1/12**.

This version of the ESI published on 23 Aug 2024 replaces the original version published on 24 July 2024. The changes made do not affect the scientific content.

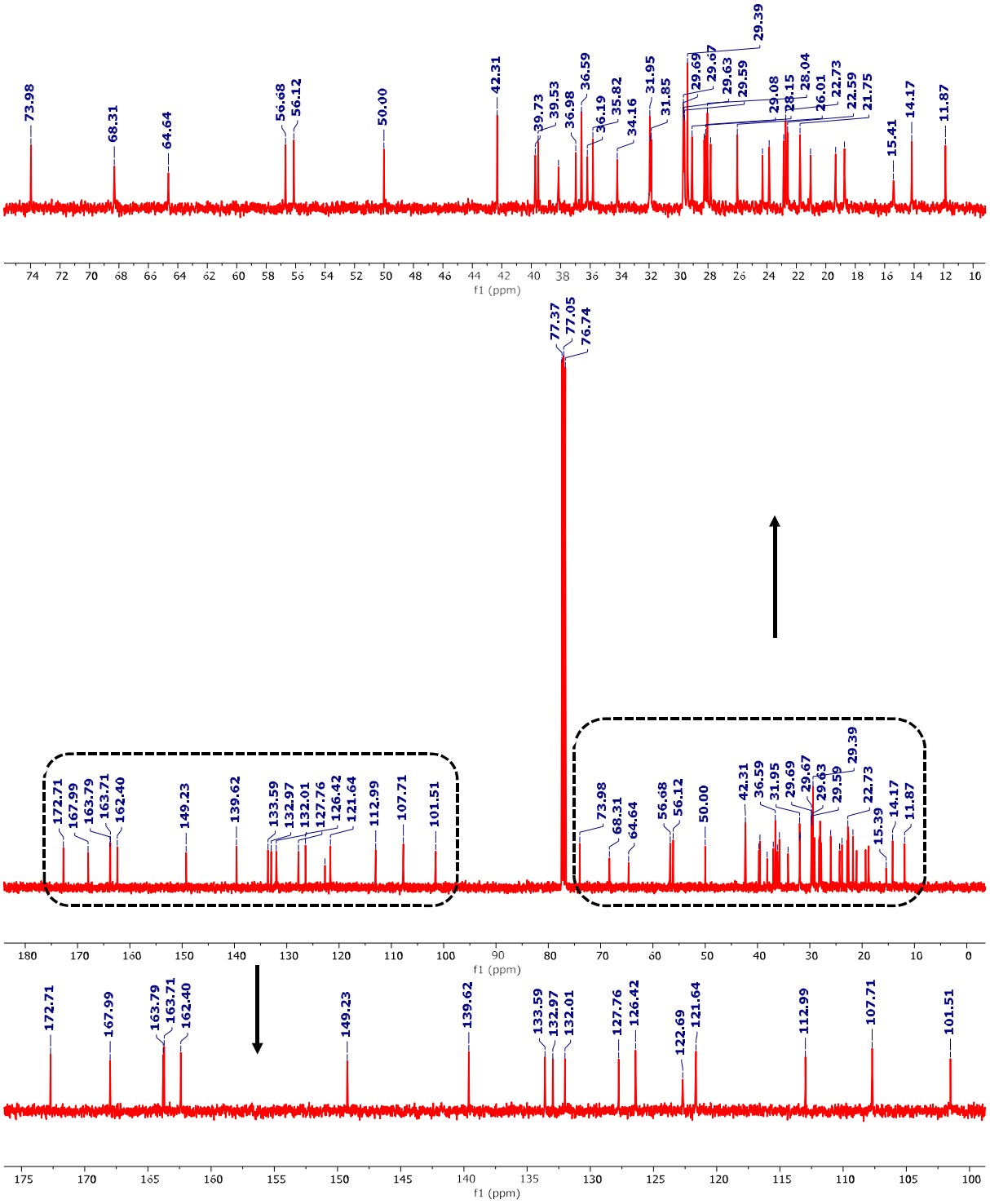

Fig. S6 ^{13}C NMR spectrum of compound **1/12**.

This version of the ESI published on 23 Aug 2024 replaces the original version published on 24 July 2024. The changes made do not affect the scientific content.

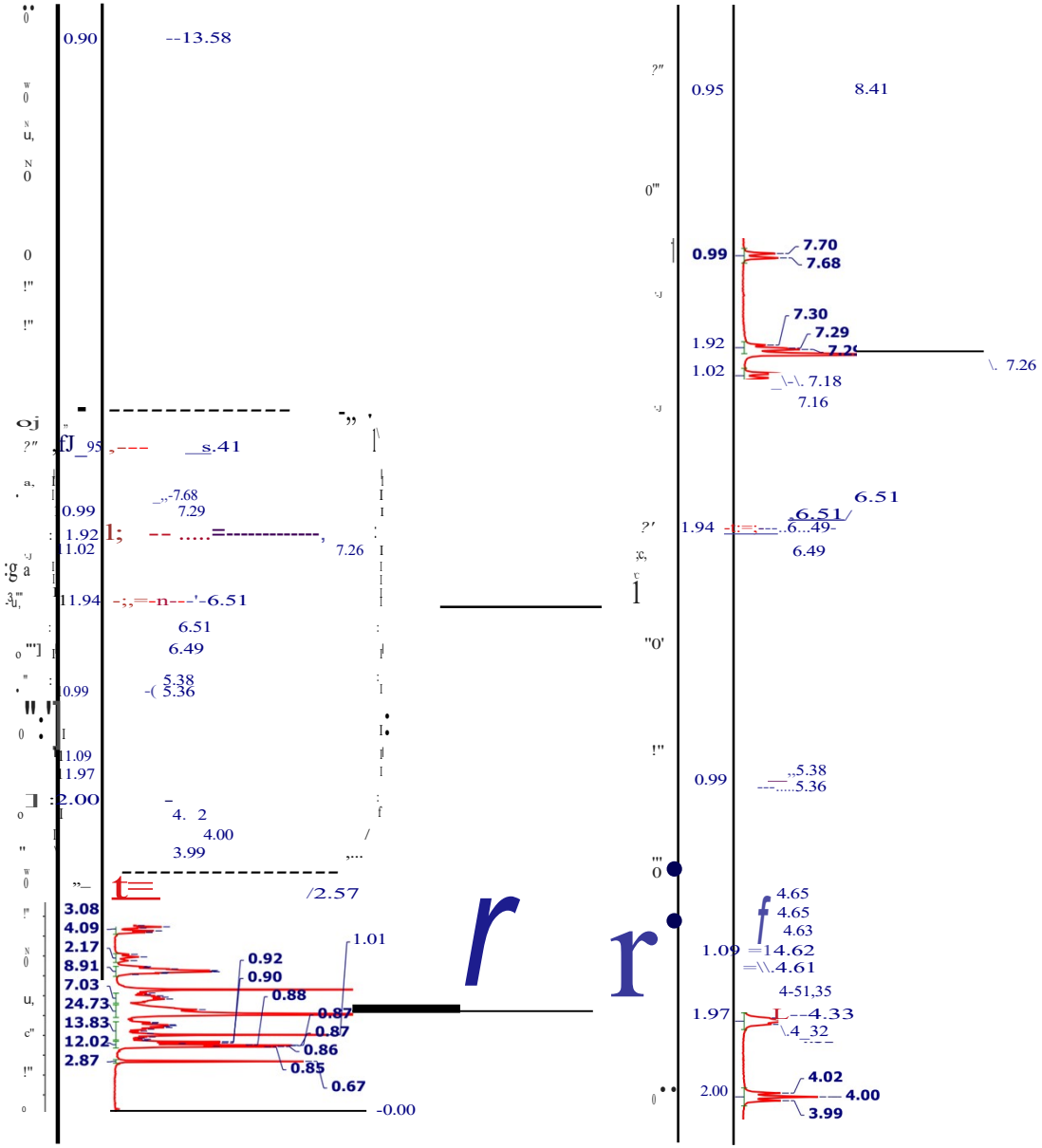

Fig. S7 ^{1}H NMR spectrum of compound **1/14**.

This version of the ESI published on 23 Aug 2024 replaces the original version published on 24 July 2024. The changes made do not affect the scientific content.

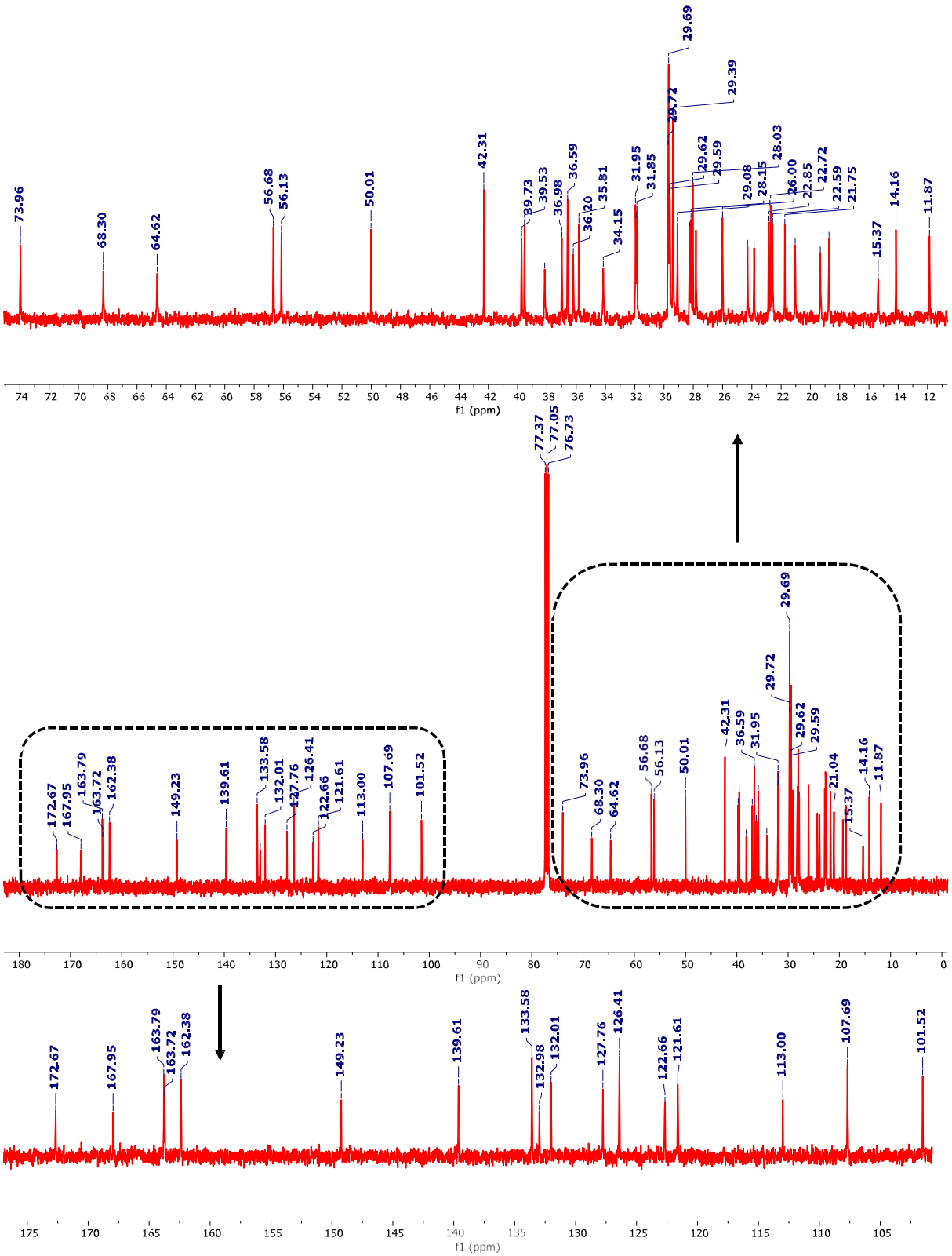

Fig. S8 ^{13}C NMR spectrum of compound **1/14**.

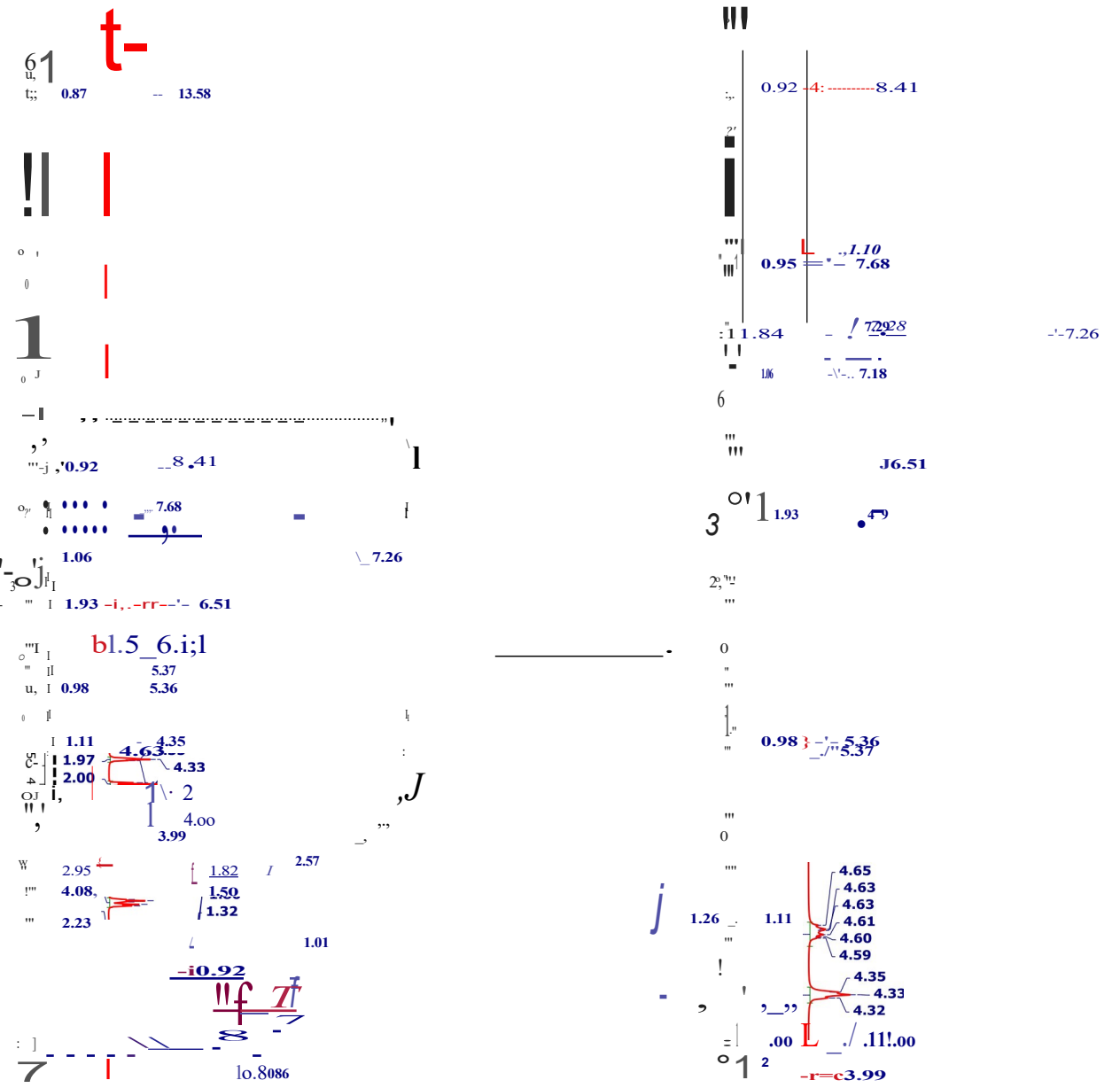

Fig. S9 ^{1}H NMR spectrum of compound **1/16**.

This version of the ESI published on 23 Aug 2024 replaces the original version published on 24 July 2024. The changes made do not affect the scientific content.

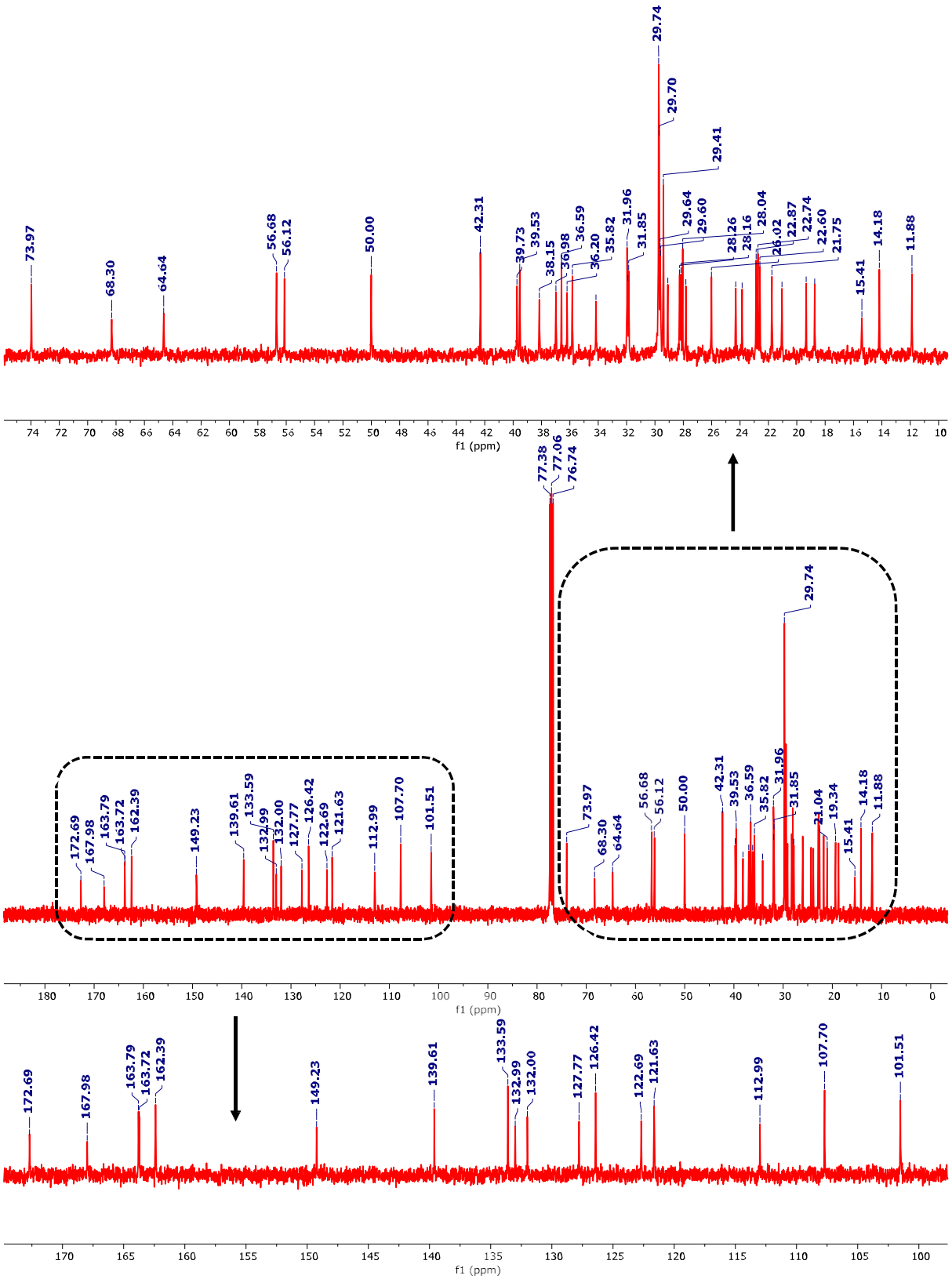

Fig. S10 ^{13}C NMR spectrum of compound **1/16**.

This version of the ESI published on 23 Aug 2024 replaces the original version published on 24 July 2024. The changes made do not affect the scientific content.

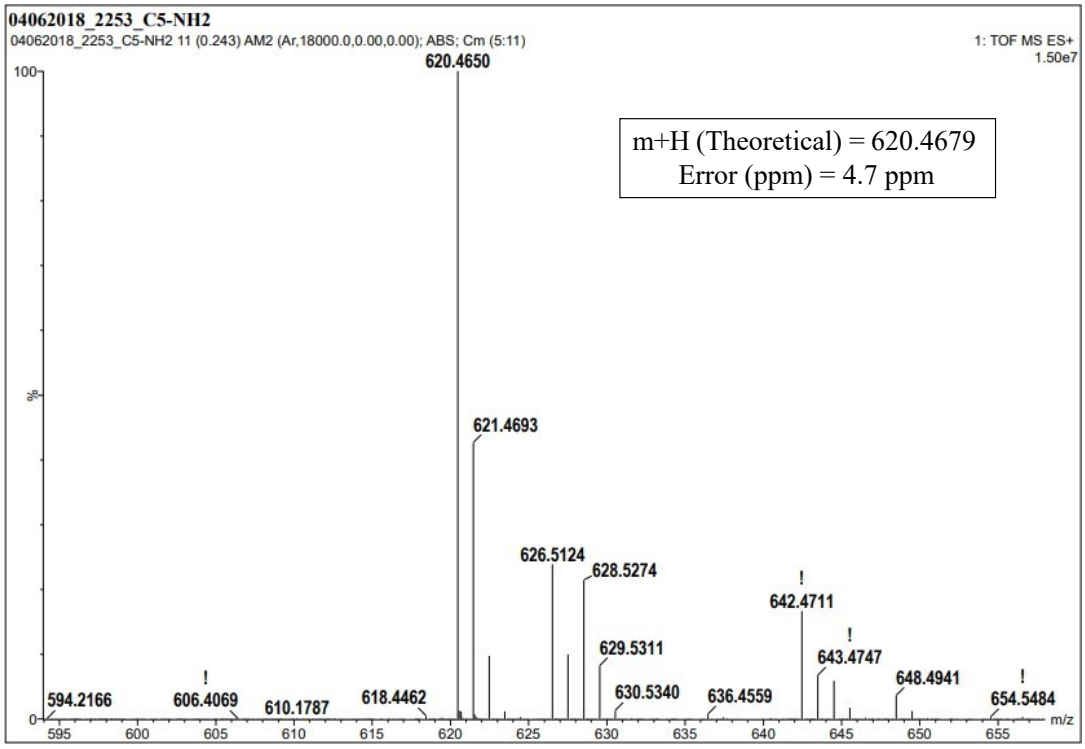

Fig. S11 ESI spectrum of **f**.

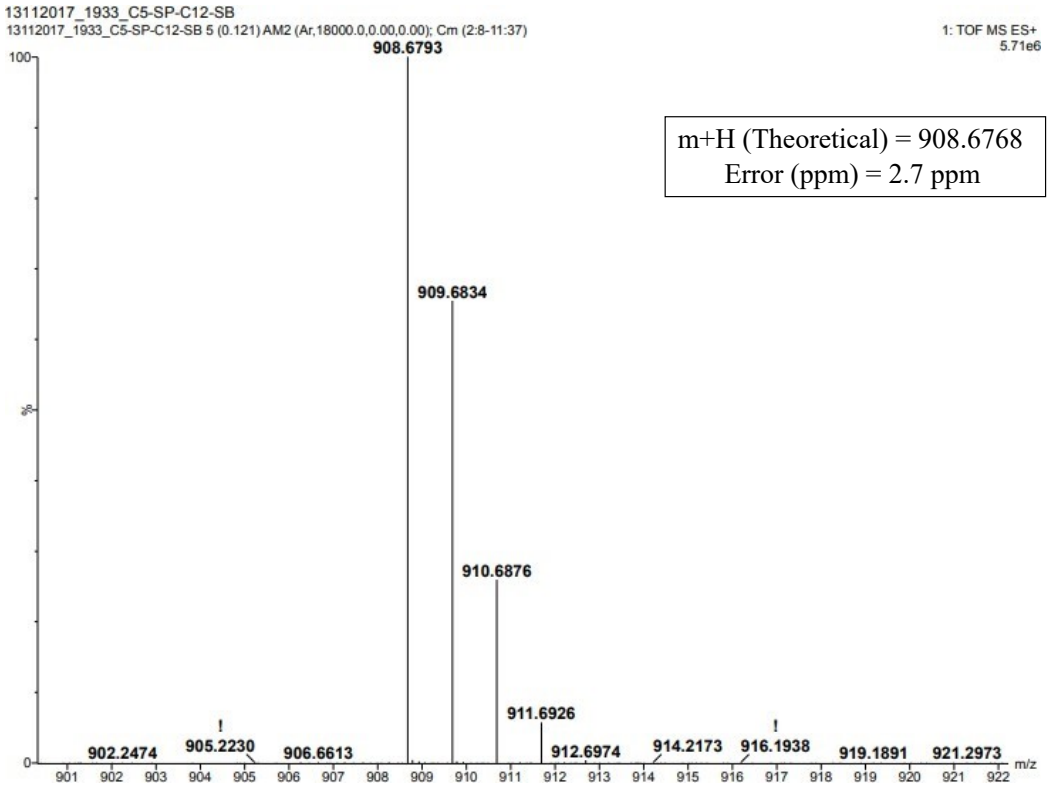

Fig. S12 ESI spectrum of **1/12**.

This version of the ESI published on 23 Aug 2024 replaces the original version published on 24 July 2024. The changes made do not affect the scientific content.

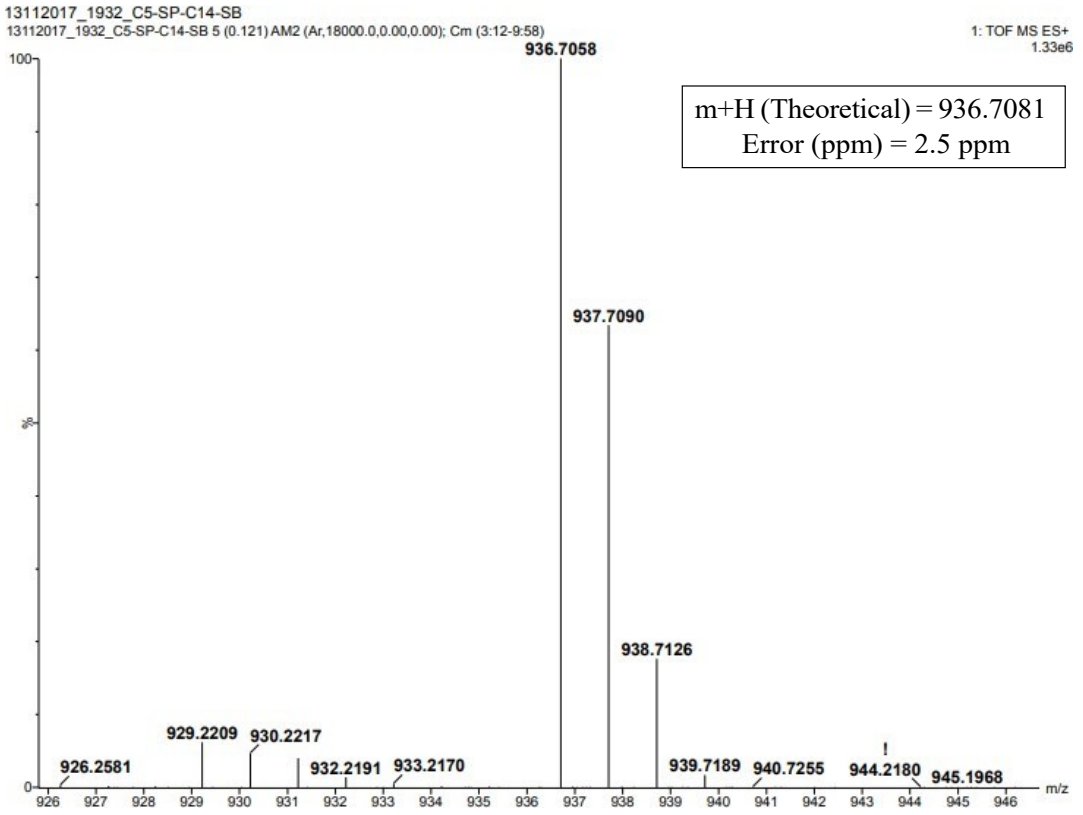

Fig. S13 ESI spectrum of **1/14**.

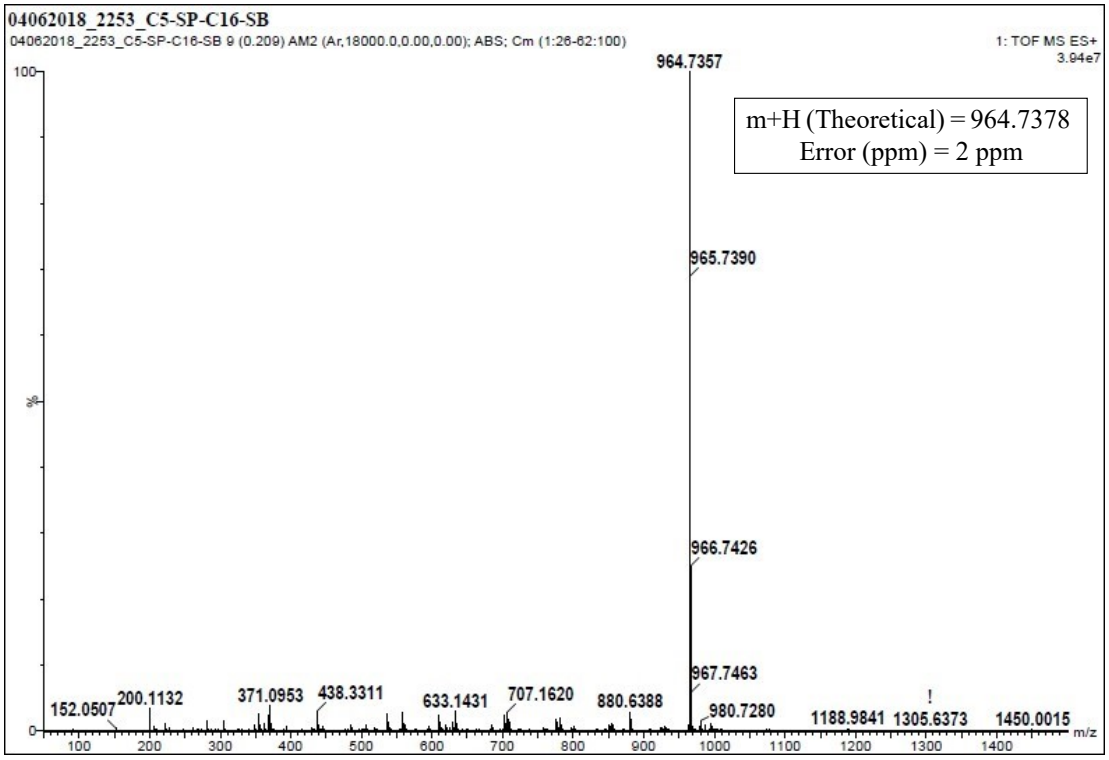

Fig. S14 ESI spectrum of **1/16**.

This version of the ESI published on 23 Aug 2024 replaces the original version published on 24 July 2024. The changes made do not affect the scientific content.

3. Attenuated Total Reflectance (ATR) studies

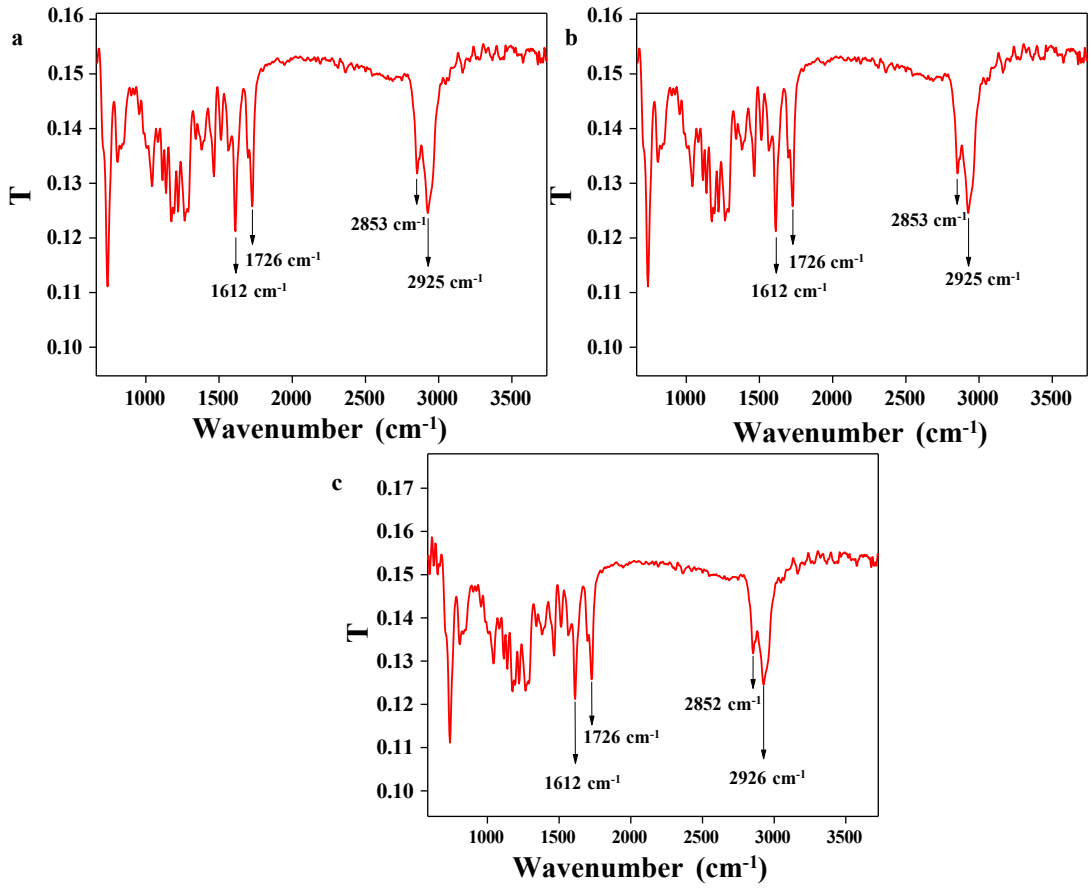

Fig. S15 IR spectrum of compound (a) **1/12** (b) **1/14** and (c) **1/16**.

4. UV-vis studies

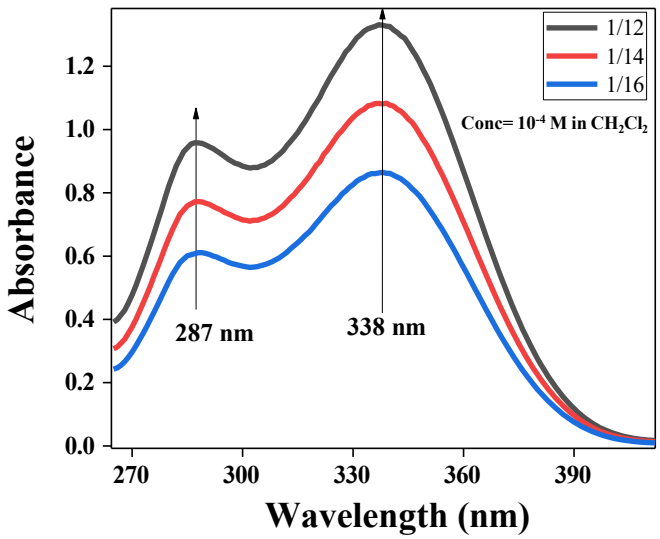

Fig. S16 UV spectra of compounds **1/12 (b) 1/14** and **1/16**.

This version of the ESI published on 23 Aug 2024 replaces the original version published on 24 July 2024. The changes made do not affect the scientific content.

5. Density Functional Theory (DFT) study

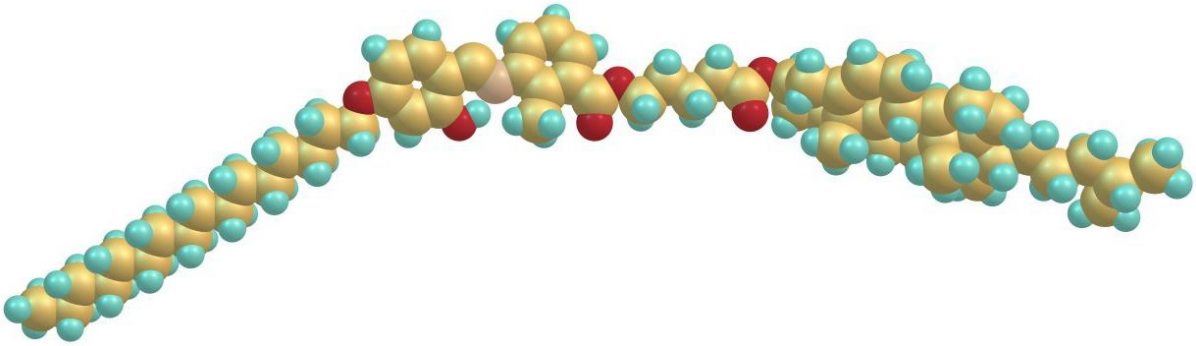

Fig. S17 DFT optimized bent-molecular architecture of the non-symmetrical cholesterol-based dimer **1/14**. (at the level of B3LYP/6-311G(d,p)), where the molecular length of the compound **1/14** is 56.0 Å.

6. Polarizing Optical Microscopy (POM) studies

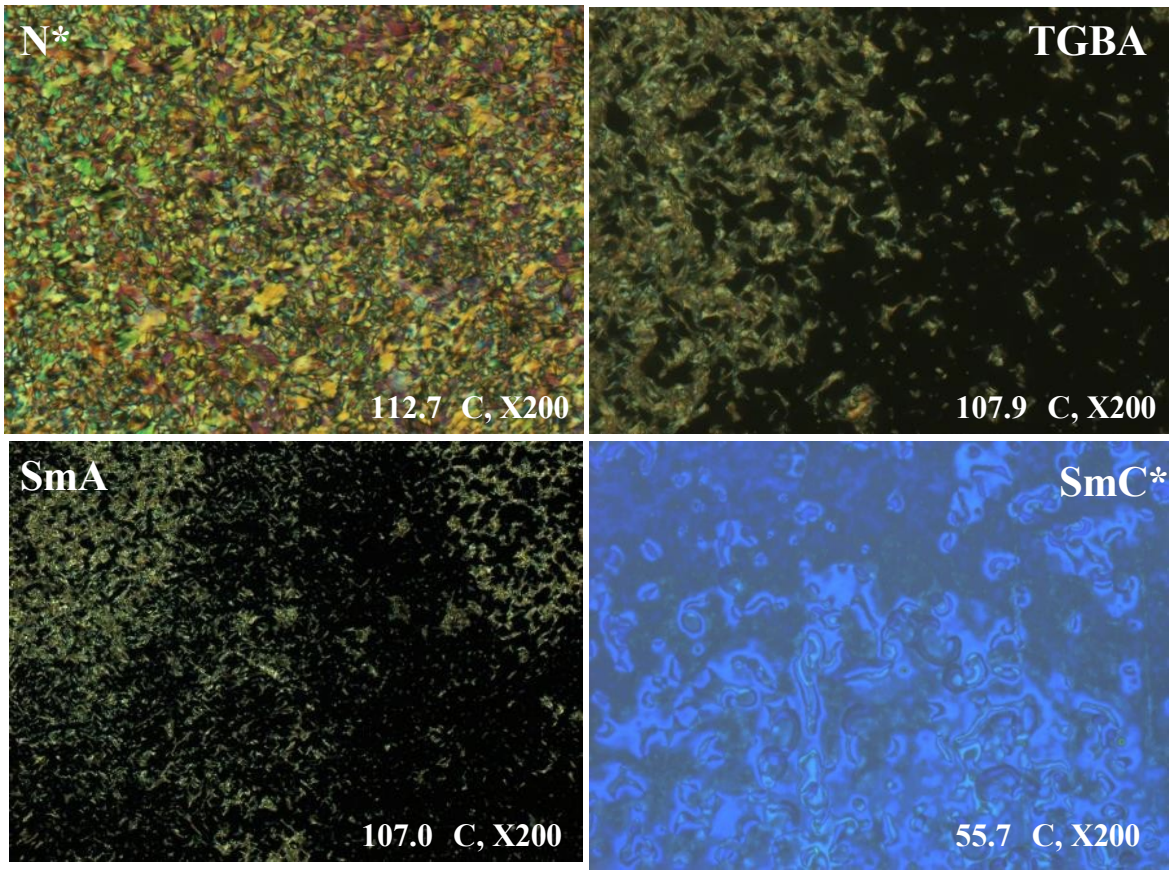

Fig. S18 POM micrographs of compound **1/14** exhibiting N*, TGBA, SmA and SmC* mesophase. The first three images (a, b, c) are captured in a normal glass slide with a coverslip. The last image d is captured in a homeotropic cell of thickness 3.3 µm.

This version of the ESI published on 23 Aug 2024 replaces the original version published on 24 July 2024. The changes made do not affect the scientific content.

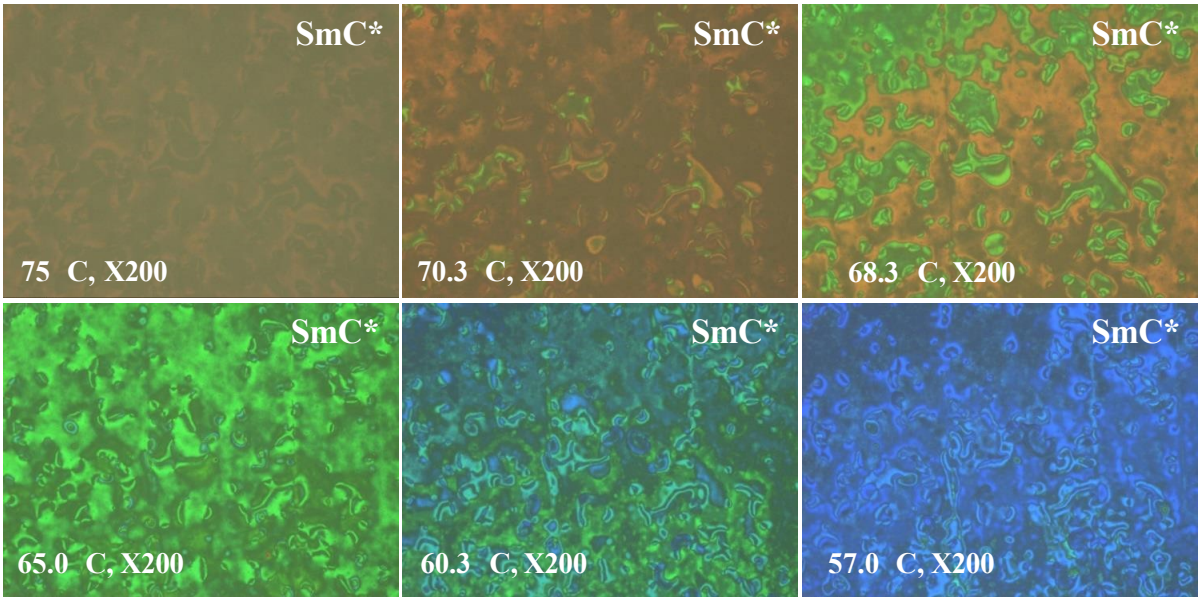

Fig. S19 POM micrographs of compound **1/14** of SmC* mesophase in a 3.3 µm ITO coated homeotropic cell. All the images are taken under crossed polarizers with a magnification of X200

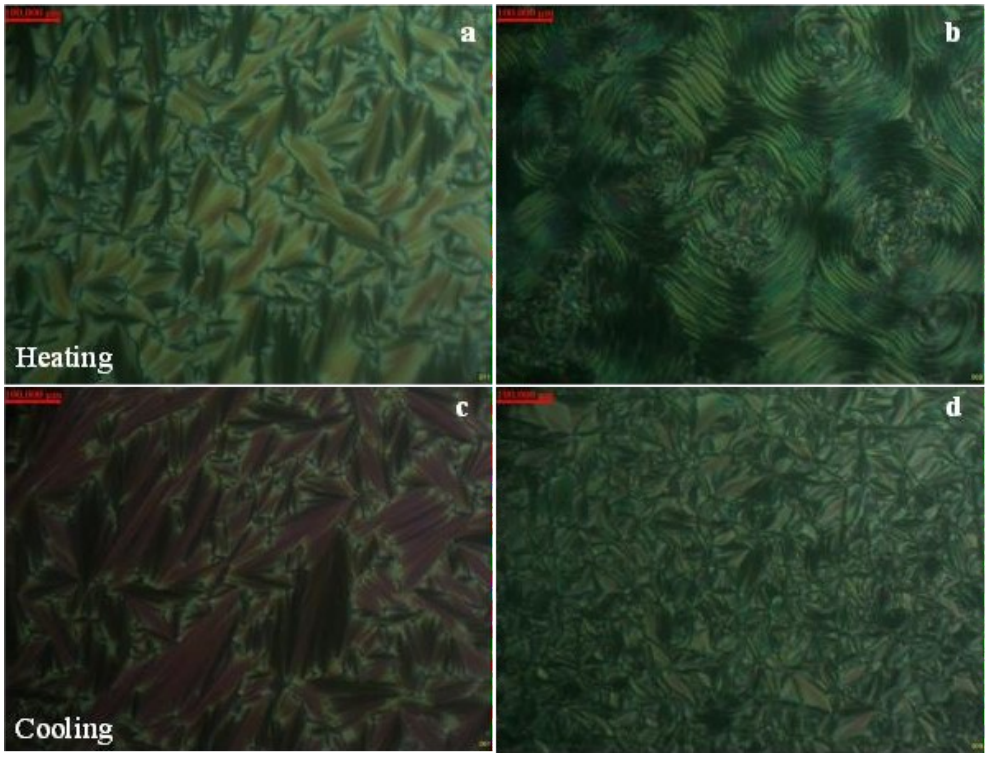

Fig. S20 POM micrographs of compound **1/14** of TGBA mesophase in the heating and cooling cycle with (a, c) homogeneous alignment (b, d) homeotropic alignment respectively. (Magnification: X400)

This version of the ESI published on 23 Aug 2024 replaces the original version published on 24 July 2024. The changes made do not affect the scientific content.

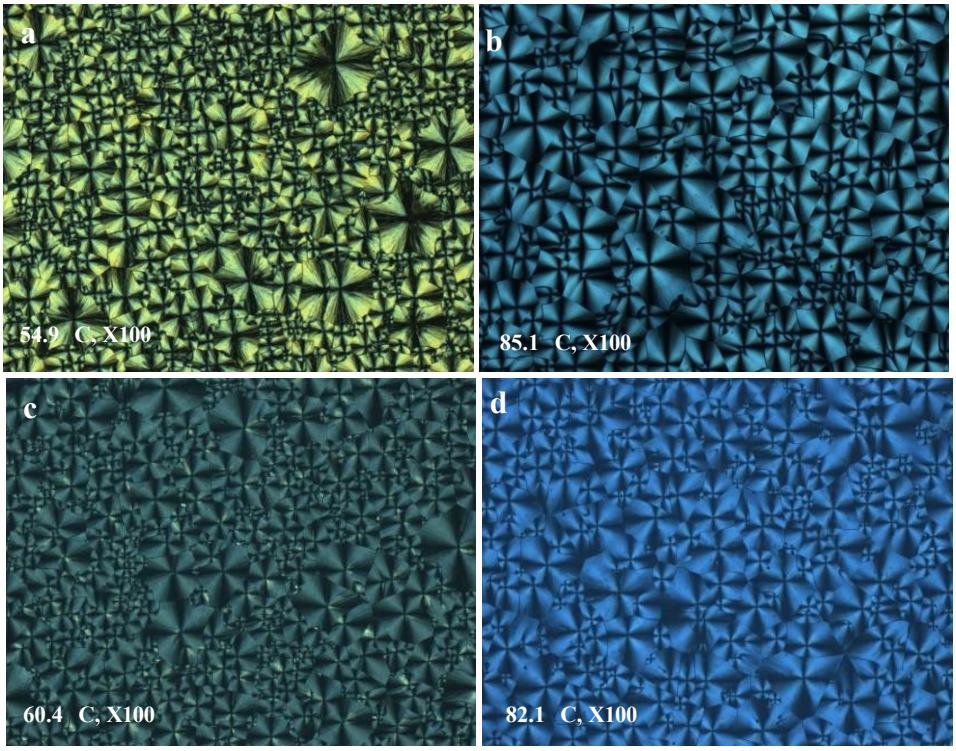

Fig. S21 Micrographic evidence of the crystal polymorphism in (a, b) normal glass slide with a coverslip and (c, d) in 5.0 μm PI-ITO coated homogeneous cell for compound **1/14**. All the images were captured under crossed polarizers with a magnification of X100.

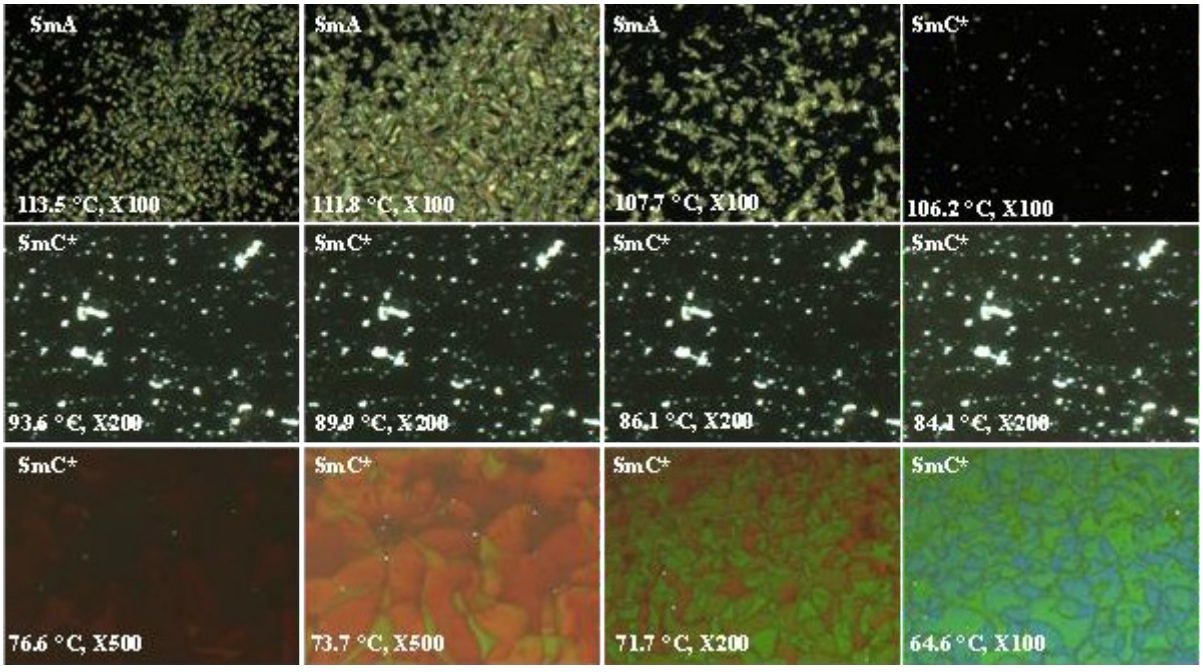

Fig. S22 POM micrographs of compound **1/16** displaying the mesophase transition from the SmA to SmC* phase in a normal glass slide with a coverslip in the cooling cycle. All the images are captured under crossed polarizers with a magnification of X200.

This version of the ESI published on 23 Aug 2024 replaces the original version published on 24 July 2024. The changes made do not affect the scientific content.

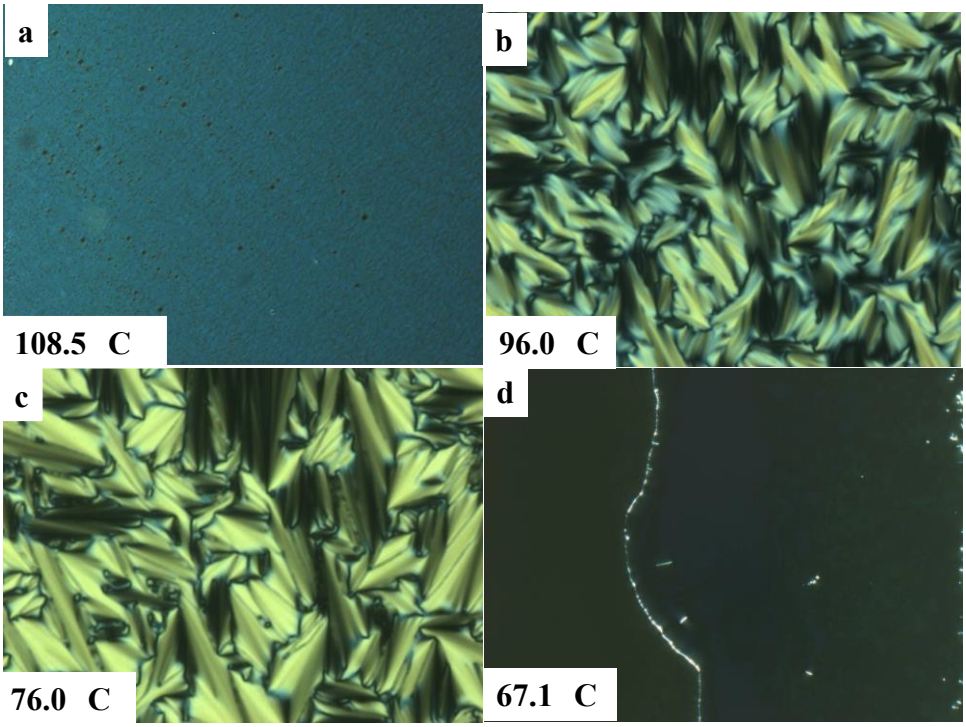

Fig. S23 POM micrographs of compound **1/12** showing the change in the mesophase transition from (a) N* (X100) in normal glass slide with a coverslip, (b) SmC* (X500), (c) SmC* (X500) in 3.2 μm PI-ITO coated homogeneous cell (cooling) and (d) SmC* (X200) in 3.3 μm ITO coated homeotropic cell (cooling). All the images are taken under crossed polarizers with a magnification of X500 and X200.

This version of the ESI published on 23 Aug 2024 replaces the original version published on 24 July 2024. The changes made do not affect the scientific content.

7. Differential Scanning Calorimetry (DSC) studies

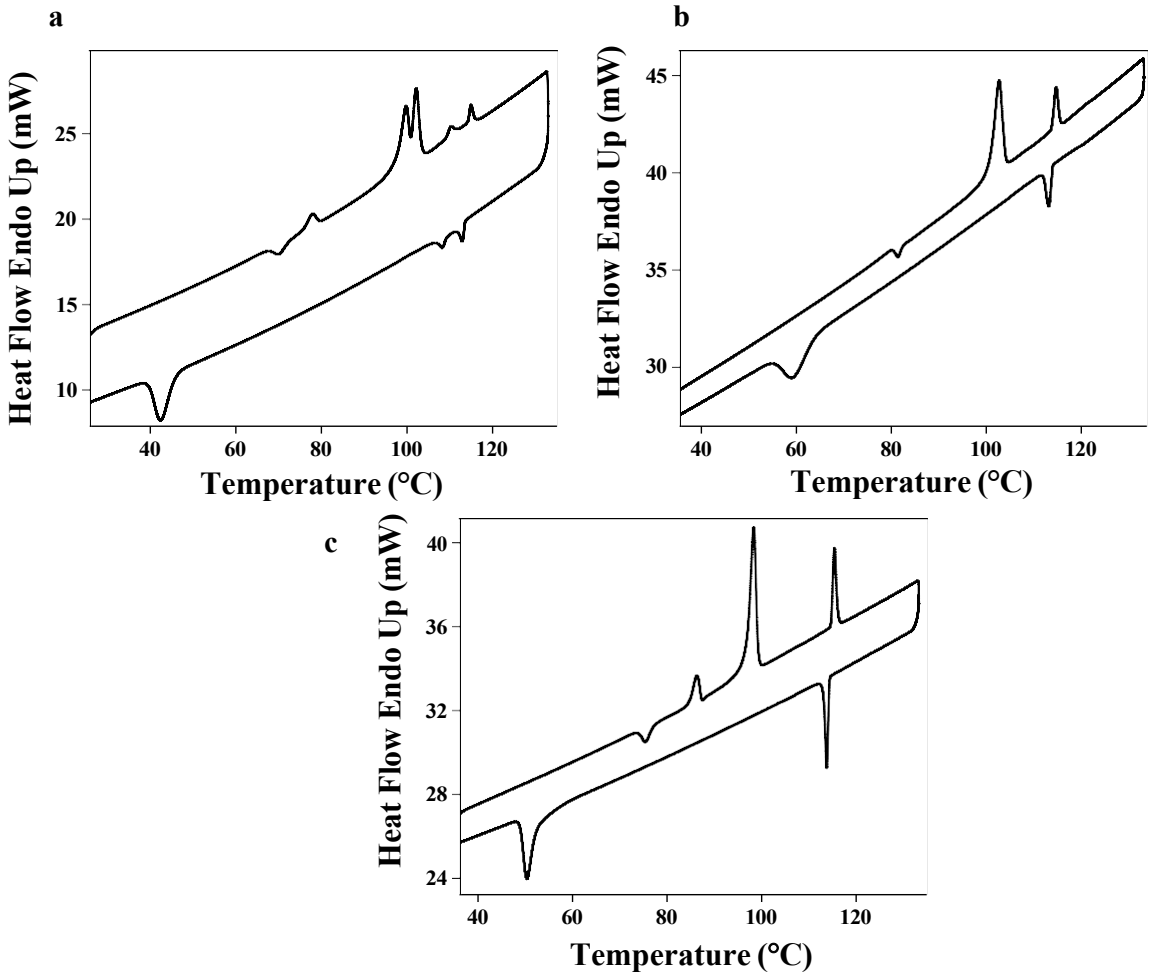

Fig. S24 DSC thermogram of compound (a) **1/12**, (b) **1/14**, (c) **1/16**.

This version of the ESI published on 23 Aug 2024 replaces the original version published on 24 July 2024. The changes made do not affect the scientific content.

8. Small-angle/Wide-angle X-ray scattering (SAXS/WAXS) studies

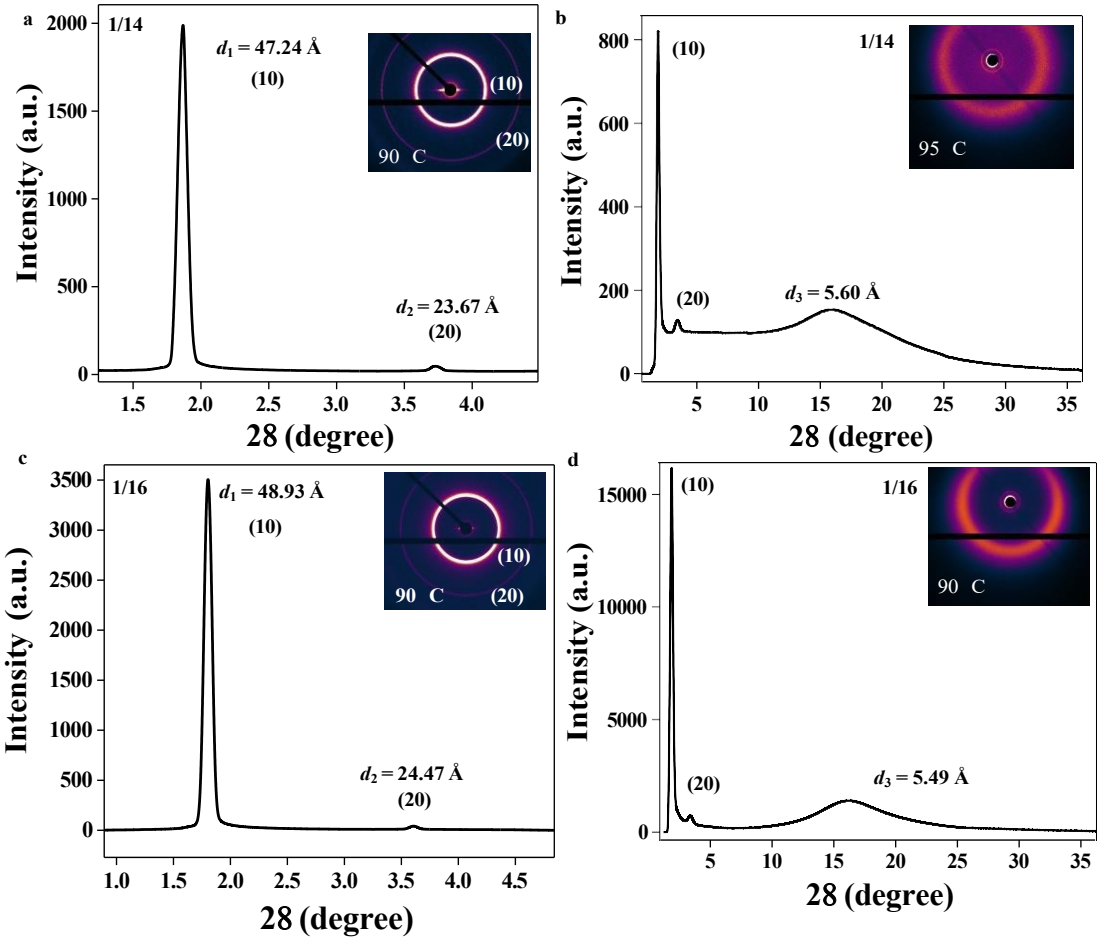

Fig. S25 The plot of Intensity *vs* 2θ for compound (a) **1/14** showing SmC* phase at a temperature of 90 °C in the small-angle region, (b) **1/14** showing SmC* phase at a temperature of 95 °C in the wide-angle region (c) **1/16** showing SmC* phase at a temperature of 90 °C in the small-angle region (d) **1/16** showing SmC* phase at a temperature of 90 °C in the wide-angle region.

This version of the ESI published on 23 Aug 2024 replaces the original version published on 24 July 2024. The changes made do not affect the scientific content.

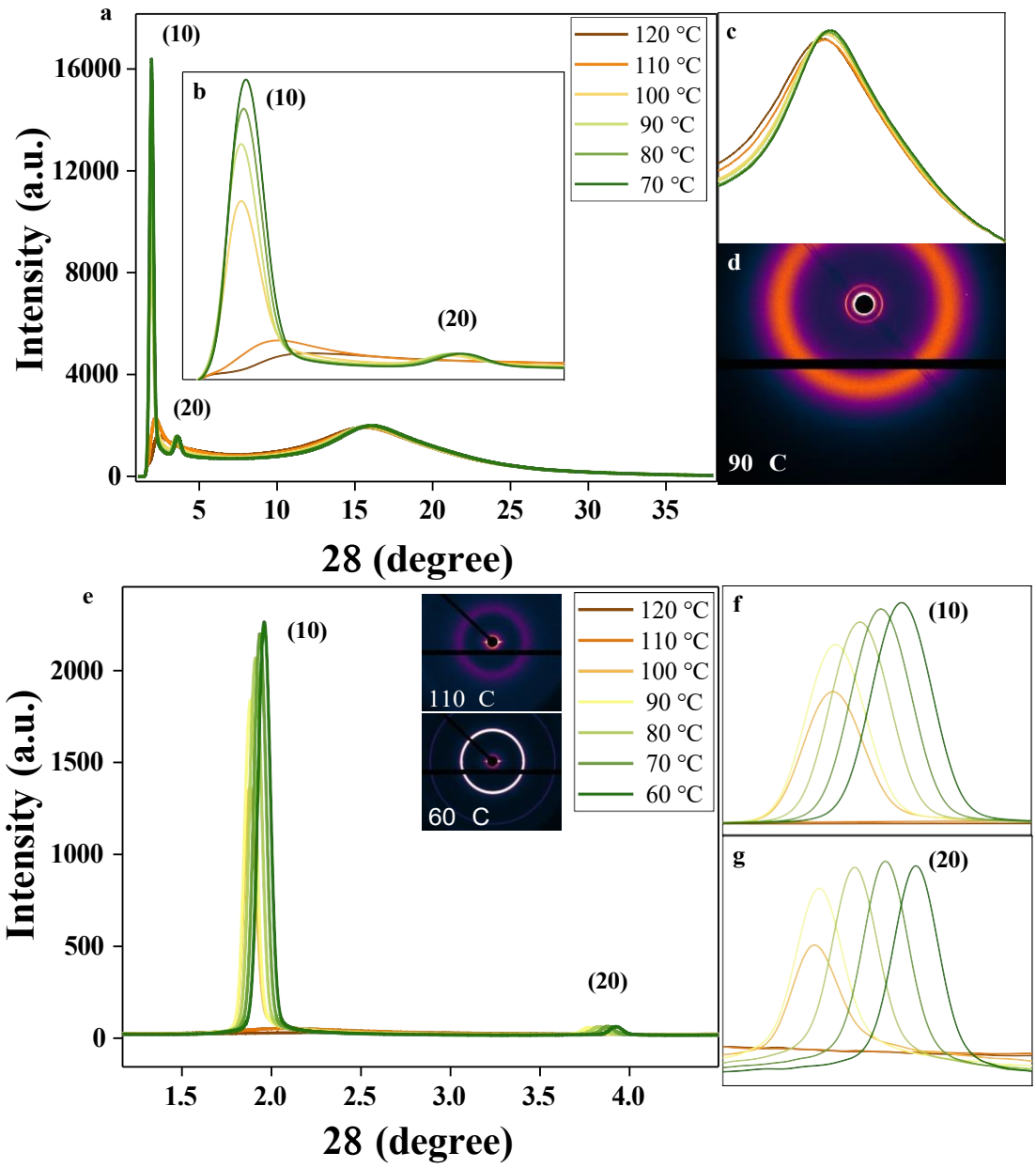

Fig. S26 (a) Temperature-dependent WAXS plot of compound **1/12** displaying three peaks: (10), (20) and a broad peak in the wide-angle region, (b) Zoomed version of two peaks (10) and (20) in the small-angle region, (c) Zoomed Version of a broad peak in the wide-angle region (d) 2D diffractogram at a temperature of 90 °C, (e) Temperature-dependent SAXS plot of compound **1/12** displaying two peaks: (10), (20) and the inset shows the 2D diffractograms at a temperature of 110 °C and 60 °C, (f) Zoomed version of (10) peak in the small-angle region, (g) Zoomed version of (20) peak in the small-angle region.

This version of the ESI published on 23 Aug 2024 replaces the original version published on 24 July 2024. The changes made do not affect the scientific content.

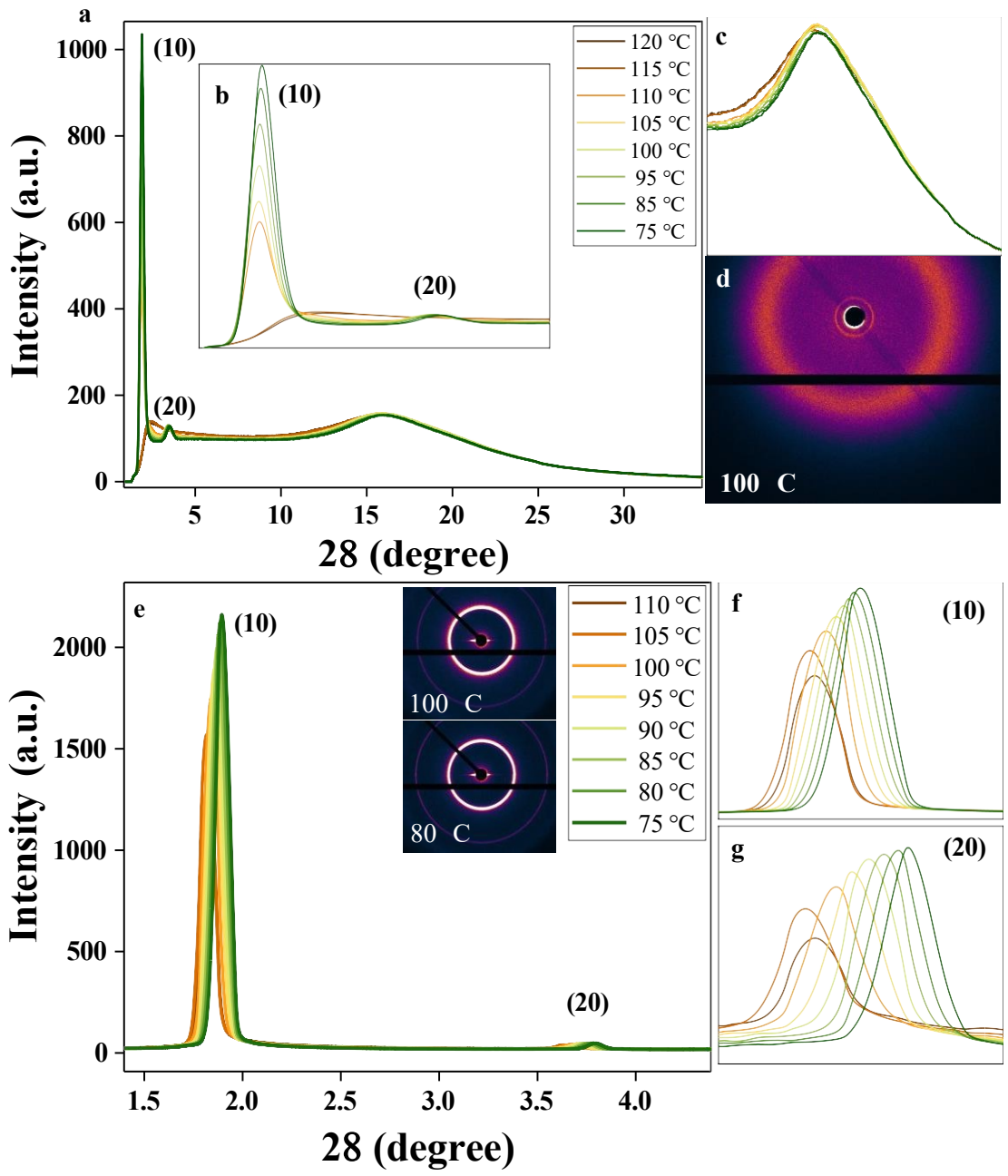

Fig. S27 (a) Temperature-dependent WAXS plot of compound **1/14** displaying three peaks: (10), (20) and a broad peak in the wide-angle region, (b) Zoomed version of two peaks (10) and (20) in the small-angle region, (c) Zoomed Version of a broad peak in the wide-angle region (d) 2D diffractogram at a temperature of 100 °C, (e) Temperature-dependent SAXS plot of compound **1/14** displaying two peaks: (10), (20) and the inset shows the 2D diffractograms at a temperature of 100 °C and 80 °C, (f) Zoomed version of (10) peak in the small-angle region, (g) Zoomed version of (20) peak in the small-angle region.

This version of the ESI published on 23 Aug 2024 replaces the original version published on 24 July 2024. The changes made do not affect the scientific content.

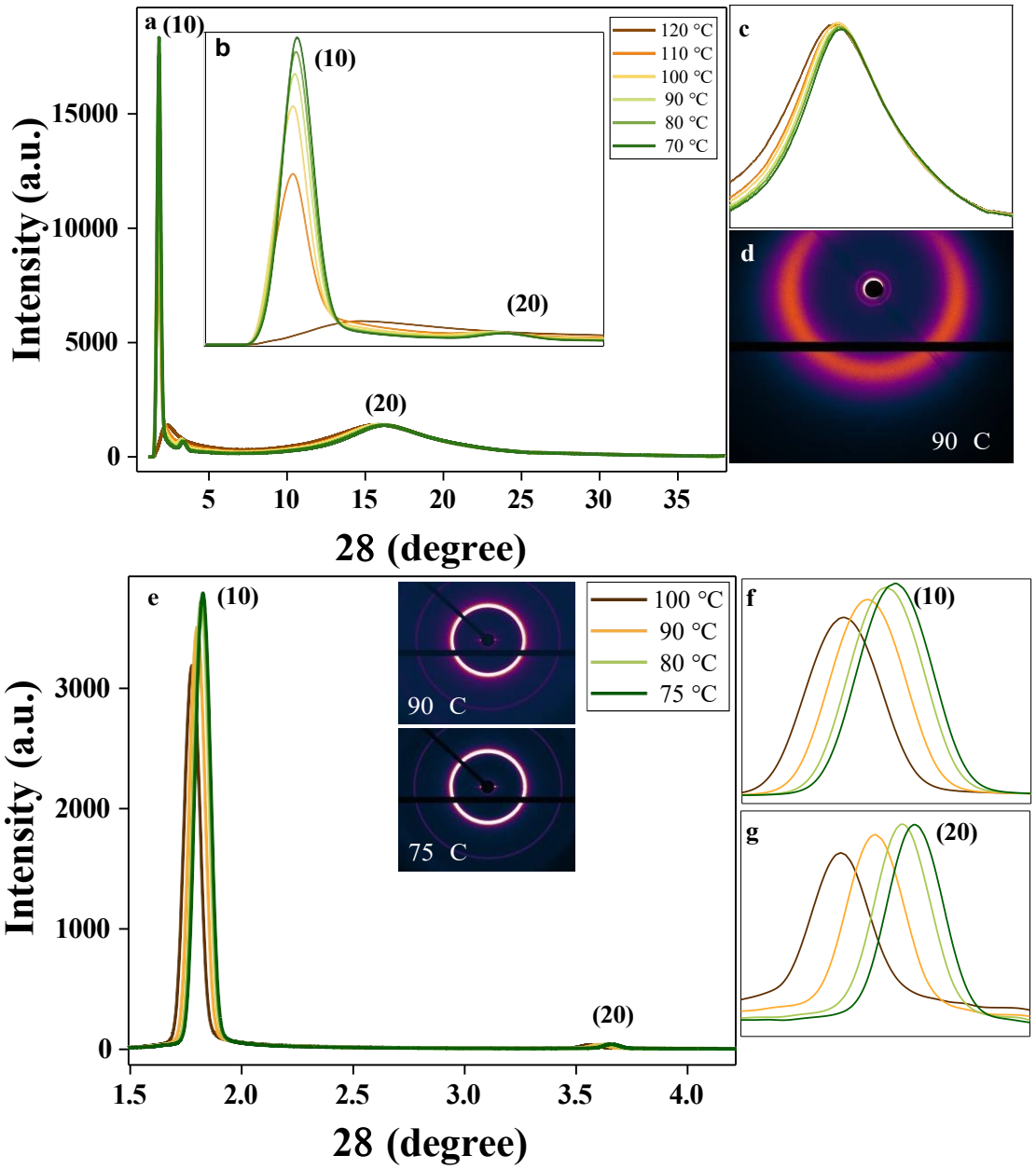

Fig. S28 (a) Temperature-dependent WAXS plot of compound **1/16** displaying three peaks: (10), (20) and a broad peak in the wide-angle region, (b) Zoomed version of two peaks i.e. (10) and (20) in the small-angle region, (c) Zoomed Version of a broad peak in the wide-angle region (d) 2D diffractogram at a temperature of 90 °C, (e) Temperature-dependent SAXS plot of compound **1/16** displaying two peaks: (10), (20) and the inset shows the 2D diffractograms at a temperature of 90 °C and 75 °C, (f) Zoomed version of (10) peak in the small-angle region, (g) Zoomed version of (20) peak in the small-angle region.

This version of the ESI published on 23 Aug 2024 replaces the original version published on 24 July 2024. The changes made do not affect the scientific content.

Table S1. Variation of the small-angle peak (d_1, in Å) and mid-angle peak (d_2, in Å), d_1-spacing [extended (ext), in Å] and tilt-angle [θ, in degree (°)] with temperature for compound **1/14**.

Temperature (°C)	d_1	d_2	Ratio (d_1/d_2)	d_1 (extended)	$\theta = \cos^{-1}(d_1 / d_{1\,(ext)})$
113	48.09		N*		
112	48.23		N*	48.29	
111	48.32	24.16	2:1 (SmA)	48.33	
110	48.40	24.20	2:1 (SmA)	48.39	
109	48.45	24.22	2:1 (SmA)	48.44	
108	48.50	24.26	2:1 (SmA)	48.49	
107	48.54	24.27	2:1 (SmA)	48.54	
106	48.58	24.28	2:1 (SmA)	48.59	1.07
105	48.58	24.28	2:1 (SmC*)	48.64	2.82
104	48.44	24.20	2:1 (SmC*)	48.69	5.80
103	48.31	24.14	2:1 (SmC*)	48.74	7.62
102	48.19	24.08	2:1 (SmC*)	48.79	9.00
101	48.09	24.04	2:1 (SmC*)	48.84	10.06
100	48.01	24.00	2:1 (SmC*)	48.89	10.90
99	47.93	23.96	2:1 (SmC*)	48.94	11.67
98	47.85	23.94	2:1 (SmC*)	48.99	12.40
97	47.77	23.87	2:1 (SmC*)	49.04	13.09
96	47.70	23.85	2:1 (SmC*)	49.09	13.69
95	47.63	23.83	2:1 (SmC*)	49.15	14.26
94	47.56	23.80	2:1 (SmC*)	49.20	14.81
93	47.51	23.77	2:1 (SmC*)	49.25	15.26
92	47.45	23.72	2:1 (SmC*)	49.30	15.73
91	47.39	23.69	2:1 (SmC*)	49.35	16.19
90	47.33	23.66	2:1 (SmC*)	49.40	16.64
89	47.27	23.64	2:1 (SmC*)	49.45	17.07
88	47.22	23.62	2:1 (SmC*)	49.50	17.45
87	47.16	23.58	2:1 (SmC*)	49.55	17.87
86	47.11	23.56	2:1 (SmC*)	49.60	18.23
85	47.06	23.56	2:1 (SmC*)	49.65	18.59
84	47.01	23.53	2:1 (SmC*)	49.70	18.94
83	46.96	23.49	2:1 (SmC*)	49.75	19.29
82	46.91	23.46	2:1 (SmC*)	49.80	19.62
81	46.86	23.43	2:1 (SmC*)	49.85	19.96
80	46.81	23.39	2:1 (SmC*)	49.90	20.28
79	46.76	23.39	2:1 (SmC*)	49.95	20.60
78	46.71	23.35	2:1 (SmC*)	50.01	20.92
77	46.67	23.33	2:1 (SmC*)	50.06	21.19

This version of the ESI published on 23 Aug 2024 replaces the original version published on 24 July 2024. The changes made do not affect the scientific content.

76	46.62	23.31	2:1 (SmC*)	50.11	21.50
75	46.57	23.28	2:1 (SmC*)	50.16	21.80
74	46.53	23.28	2:1 (SmC*)	50.21	22.07
73	46.48	23.24	2:1 (SmC*)	50.26	22.36
72	46.43	23.21	2:1 (SmC*)	50.31	22.65
71	46.38	23.19	2:1 (SmC*)	50.36	22.93
70	46.33	23.18	2:1 (SmC*)	50.41	23.21
69	46.28	23.15	2:1 (SmC*)	50.46	23.49

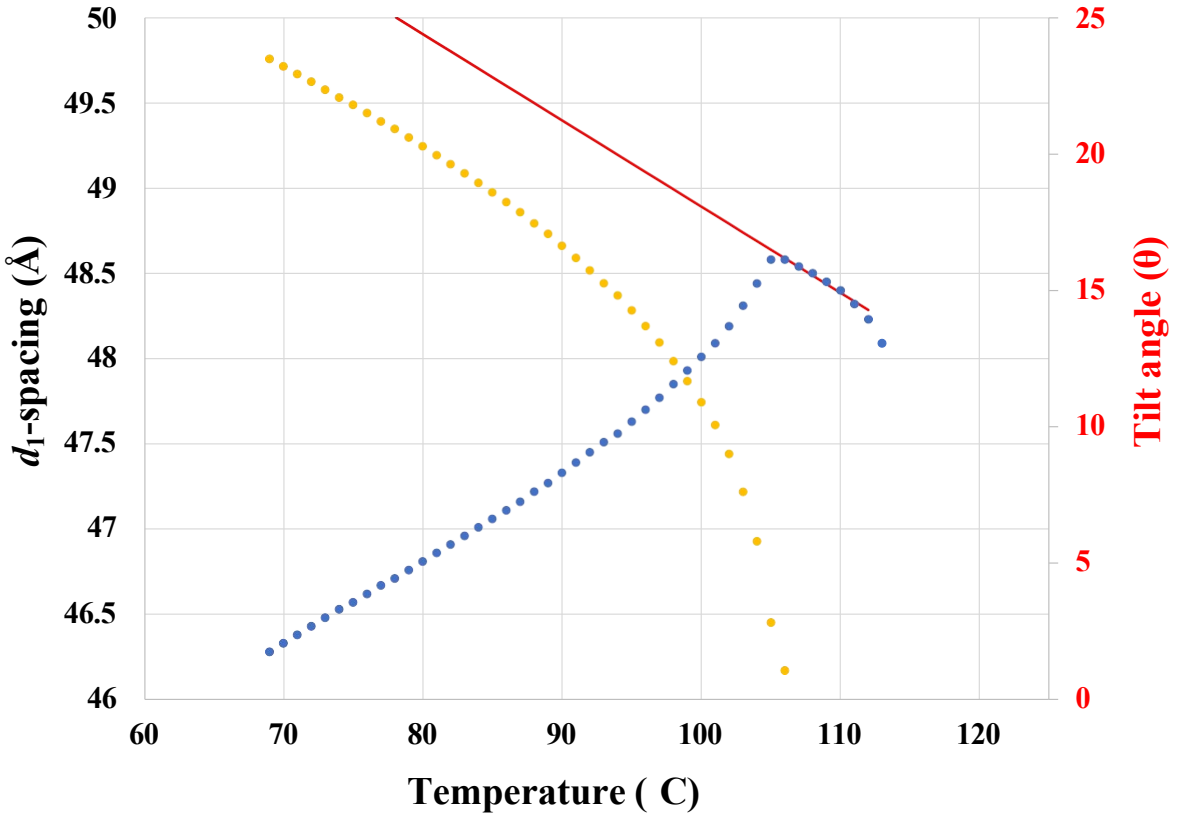

Fig. S29 Plot of d_1-spacing, d_1-spacing (extended), tilt angle with temperature for compound **1/14**, where the blue curve denotes variation of d_1-spacing with temperature, red curve denotes variation of d_1-spacing (extended) with temperature and the yellow curve denotes variation of tilt angle with temperature.

Table S2. Variation of the small-angle peak (d_1, in Å) and mid-angle peak (d_2, in Å), d_1-spacing [extended (ext), in Å] and tilt-angle [θ, in degree (°)] with temperature for compound **1/16**.

Temperature (°C)	d_1	d_2	Ratio (d_1/d_2)	d_1 (extended)	$\theta = \cos^{-1}(d_1 / d_{1\,(ext)})$
114	49.89	24.98	2:1 (SmA)	49.97	
113	49.89	25.03	2:1 (SmA)	50.03	
112	50.07	25.06	2:1 (SmA)	50.08	
111	50.15	25.07	2:1 (SmA)	50.14	

110	50.21	25.11	2:1 (SmA)	50.20	
109	50.26	25.14	2:1 (SmA)	50.25	
108	50.3	25.16	2:1 (SmA)	50.31	1.25
107	50.29	25.15	2:1 (SmC*)	50.37	3.21
106	50.12	25.06	2:1 (SmC*)	50.43	6.31
105	49.97	24.98	2:1 (SmC*)	50.48	8.17
104	49.85	24.92	2:1 (SmC*)	50.54	9.48
103	49.74	24.87	2:1 (SmC*)	50.60	10.56
102	49.65	24.83	2:1 (SmC*)	50.65	11.43
101	49.56	24.77	2:1 (SmC*)	50.71	12.23
100	49.48	24.75	2:1 (SmC*)	50.77	12.93
99	49.41	24.69	2:1 (SmC*)	50.83	13.55
98	49.33	24.68	2:1 (SmC*)	50.88	14.19
97	49.27	24.64	2:1 (SmC*)	50.94	14.71
96	49.20	24.61	2:1 (SmC*)	51.00	15.25
95	49.14	24.55	2:1 (SmC*)	51.05	15.73
94	49.08	24.52	2:1 (SmC*)	51.11	16.20
93	49.02	24.52	2:1 (SmC*)	51.17	16.66
92	48.97	24.48	2:1 (SmC*)	51.22	17.06
91	48.91	24.47	2:1 (SmC*)	51.28	17.49
90	48.86	24.44	2:1 (SmC*)	51.34	17.87
89	48.81	24.41	2:1 (SmC*)	51.39	18.25
88	48.76	24.39	2:1 (SmC*)	51.45	18.62
87	48.72	24.36	2:1 (SmC*)	51.51	18.94
86	48.67	24.34	2:1 (SmC*)	51.57	19.29
85	48.62	24.32	2:1 (SmC*)	51.62	19.64
84	48.5	24.29	2:1 (SmC*)	51.68	19.98
83	48.53	24.26	2:1 (SmC*)	51.74	20.28
82	48.48	24.24	2:1 (SmC*)	51.79	20.61
81	48.44	24.23	2:1 (SmC*)	51.85	20.90
80	48.39	24.21	2:1 (SmC*)	51.91	21.21
79	48.35	24.18	2:1 (SmC*)	51.97	21.50
78	48.31	24.16	2:1 (SmC*)	52.02	21.77
77	48.26	24.14	2:1 (SmC*)	52.08	22.08
76	48.22	24.12	2:1 (SmC*)	52.14	22.35
75	48.18	24.10	2:1 (SmC*)	52.19	22.61
74	48.13	24.08	2:1 (SmC*)	52.25	22.91
73	48.09	24.05	2:1 (SmC*)	52.31	23.16
72	48.05	24.03	2:1 (SmC*)	52.36	23.42
71	48.01	24.00	2:1 (SmC*)	52.42	23.67
70	47.97	24.00	2:1 (SmC*)	52.48	23.92

This version of the ESI published on 23 Aug 2024 replaces the original version published on 24 July 2024. The changes made do not affect the scientific content.

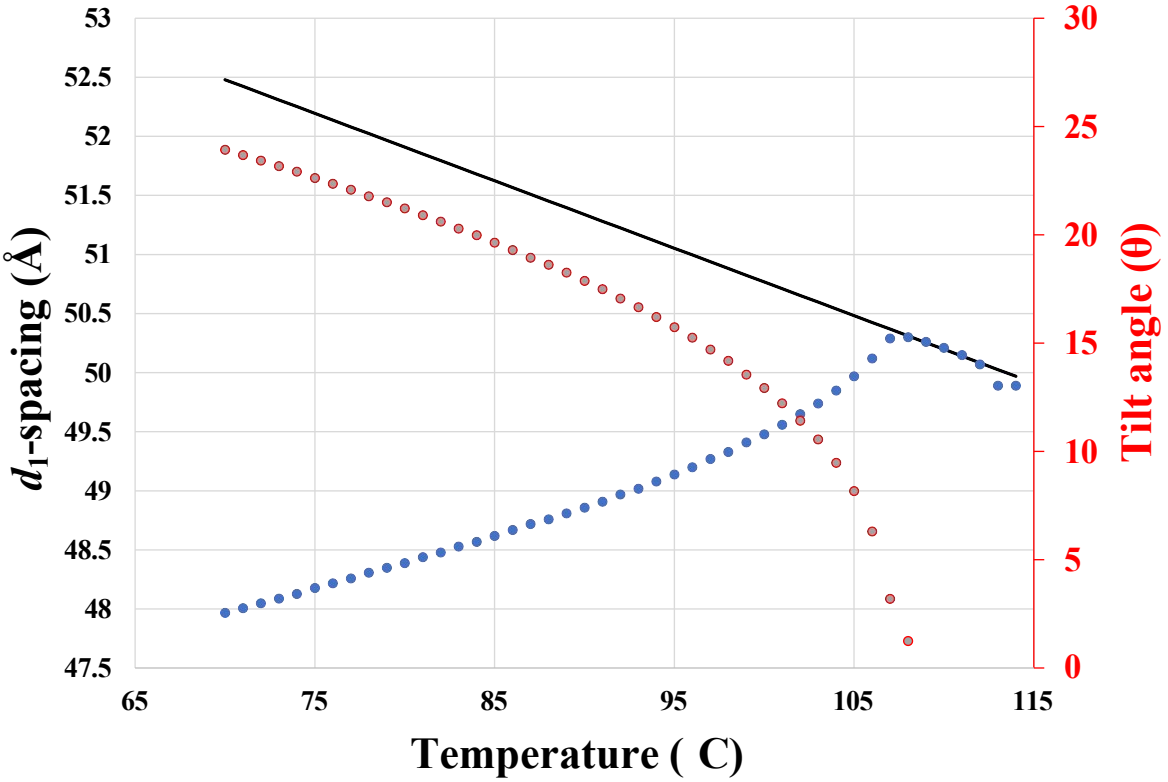

Fig. S30 Plot of d_1-spacing, d_1-spacing (extended), tilt angle with temperature for compound **1/16**, where blue curve denotes variation of d_1-spacing with temperature, black curve denotes variation of d_1-spacing (extended) with temperature and the red curve denotes variation of tilt angle with temperature.

This version of the ESI published on 23 Aug 2024 replaces the original version published on 24 July 2024. The changes made do not affect the scientific content.

9. Circular Dichroism (CD) studies

Table S3. CD spectral data of the SmC* phase exhibited by the compound **1/14** and **1/16**.

Compound	LC phase	Temperature (°C)	CD	
			λ_{max} (nm)	CD (mdeg)
1/14	SmC*	60	398, 340	1468, -29
		63	398, 340	1261, -20
		66	398, 340	1042, -14
		69	398, 340	929, 9
		72	398, 340	756, 24
		75	398, 340	626, 95
1/16	SmC*	52	361, 303	-1158, -326
		55	361, 303	-961, -337
		60	361, 303	-845, -311
		65	361, 302	-735, 282
		70	361, 302	-626, -246
		75	361, 301	-500, -195

1/14: The CD spectra could not be seen in the N*, TGBA and SmA phase as theses phases are short-lived. Here the CD signals are due to the helicoidal structure (handedness) of the SmC* phase, **1/16**: This compound has SmA and SmC* phases; the signals are due to helicoidal structure (handedness) as well as the selective reflection of the SmC* phase.

10. Instrumental Details

The details of the characterization techniques have been published elsewhere.[1,2] Briefly, the details are the following. “Structural characterization of the compound was carried out through a combination of ^{1}H-NMR and ^{13}C-NMR (Bruker Biospin Switzerland Avance-iii 400 MHz), NMR spectra were recorded using deuterated chloroform. $CDCl_3$ was used as solvent and tetramethylsilane (TMS) as an internal standard. ATR (FT-IR BRUKER-ALPHA BRUKER-1227-3513), UV-VIS-NIR spectrophotometer (LABINDIA UV-Vis Spectrophotometer 3000+), and Mass Spectrometry (Waters synapt g2s) were also performed. POM textural observations of the mesophase were performed with a Nikon Eclipse LV100POL polarizing microscope provided with a Linkam heating stage (LTS 420). DSC measurements were performed on Perkin Elmer DSC 8000 coupled to a Controlled Liquid Nitrogen Accessory (CLN_2) with a scan rate of 10 °C/min. X-ray Diffraction (XRD) studies were carried out on the

This version of the ESI published on 23 Aug 2024 replaces the original version published on 24 July 2024. The changes made do not affect the scientific content.

samples using CuK_{α} (λ=1.54 Å) radiation from GeniX3D micro source, using Pilatus 200K detector in Xeuss 2.0 SAXS/WAXS system. Circular Dichroism (CD) spectra of the samples (thin-films) were recorded under the nitrogen atmosphere on a J-820 spectropolarimeter (JASCO Ltd., Tokyo, Japan) equipped with a programmable hot stage (Mettler Toledo FP90). Newly procured rectangular quartz plates of dimensions 2 cm x 2 cm and 2 mm thickness were used for the cell fabrication. The physical parameters which include the static permittivity and broadband dielectric spectroscopy were carried out in commercially available homogeneous and homeotropic cells of thickness ~5 μm. The LC cells were placed in a heating and cooling stage HCS 302 (Instec, USA) connected to a programmable temperature controller mK1000 (Instec, U.S.A.) that controls and measures the temperature with an accuracy of 0.1 °C min^{-1}. The static permittivity values and broadband spectroscopy measurements were carried out using a precession impedance analyzer Agilent 4294A with a relative accuracy of 0.08%. A picotest G100A waveform generator was used for the electro-optical measurements in addition to an amplifier F20A (FLCE, Sweden). Agilent Digital Storage Oscilloscope (DSO X2000A), Hot stage HCS302 and temperature-controller (programmable mK1000 temperature controller, Instec, USA) were also used for electro-optical measurements."

11. References

1. V. Punjani, G. Mohiuddin, S. Kaur, R. K. Khan, S. Ghosh and S. K. Pal, *Chem. Commun.,* 2018, **54**, 3452-3455.

2. V. Punjani, G. Mohiuddin, S. Kaur, A. R. Choudhury, S. Paladugu, S. Dhara, S. Ghosh and S. K. Pal, *Chem. Eur. J.*, 2020, **26**, 5859-5871.

3. M. Gupta and S. K. Pal, *Liq. Cryst.*, 2015, **42**, 1250-1256.